AN ANALYTIC INVESTIGATION FOR SOLUTIONS OF FLOW PROPERTIES INSIDE THE SHOCK LAYER OF A SUPERSONIC FLOW PAST A CIRCULAR CYLINDER

by

Clarence Ming-Chieh Chen

Thesis submitted to the Graduate Faculty of the

Virginia Polytechnic Institute

in candidacy for the degree of

MASTER OF SCIENCE

in

AEROSPACE ENGINEERING

Approved

Chairman, F. R. DeJarnette

W. P. Harrison, Jr.

W. Emory Pace

April, 1966

Blacksburg, Virginia

I. TABLE OF CONTENTS

II. LIST OF FIGURES

Page

III. LIST OF SYMBOLS

a_m	vector defined by Eq. (5)
b	normal shock location measured from the center of cylinder (see Fig. 7)
b_m	vector defined by Eq. (5)
d_m	vector defined by Eq. (5)
e_x, e_y	unit vectors in the x and y directions, respectively (see Fig. 1)
f	freestream Mach number function defined by Eq. (68)
g	freestream Mach number function defined by Eq. (72)
K	body curvature
$\overline{K}$	nondimensionalized body curvature, KL
L	arbitrary nondimensionalizing length
M	Mach number
P	pressure
$\overline{P}$	nondimensionalized pressure, $P/\rho_\infty V_\infty^2$
R	radius of cylinder
r	radial distance measured from the center of cylinder to point in the flow field ($r = R + y$ in Fig. 1)
$\hat{r}$	perpendicular distance from body axis to point in the flow field (see Fig. 1)
u	x-direction component of local velocity (see Fig. 1)
$\overline{u}$	nondimensionalized velocity component in the x-direction, u/V_∞
v	y-direction component of local velocity (see Fig. 1)
$\overline{v}$	nondimensionalized velocity component in the y direction, v/V_∞
$\vec{V}$	local velocity vector (used in Eqs. (1) through (3) only)

V	total local velocity (see Fig. 1)	
$\bar{V}$	nondimensionalized local velocity, v/V_∞	
$\bar{V}_m$	maximum speed constant defined by Eq. (34)	
x	coordinate along body surface	(see Fig. 1)
y	coordinate normal to body surface	
$\bar{x}$	nondimensionalized x coordinate, x/L	
$\bar{y}$	nondimensionalized y coordinate, y/L	
x	mesh spacing in x direction	(see Fig. 2)
y	mesh spacing in y direction	
$\bar{x}$	nondimensionalized mesh spacing in x direction, x/L	
$\bar{y}$	nondimensionalized mesh spacing in y direction, y/L	
$(\Delta\bar{y})_{max}$	maximum $\Delta\bar{y}$ value defined by Eq. (61)	
γ	ratio of specific heats (= 1.4 for air)	
δ	shock stand-off distance (see Fig. 7)	
θ	angle between local body tangent and horizontal axis of symmetry (see Fig. 1)	
λ_x	scale factor in x direction, defined by Eq. (6)	
ξ	pressure ratio defined by Eq. (26)	
ξ_{max}	value of ξ defined by Eq. (51)	
ρ	density	
$\bar{\rho}$	nondimensionalized density, ρ/ρ_∞	
σ	function defined by Eq. (27)	
τ	mesh spacing ratio defined by Eq. (28)	
τ_{min}	minimum value of τ defined by Eq. (43)	
τ^*	sonic value of τ defined by Eq. (58)	

Φ velocity potential

ω $90^{o} - \theta$

Subscripts:

$\left.\begin{matrix} 11 \\ 13 \\ 22 \\ 31 \end{matrix}\right\}$ particular mesh points (see Fig. 2)

k, ℓ positive integers denoting lines of constant x and y, respectively (see Fig. 2)

N.S. on immediate downstream side of normal shock

stag stagnation point condition

∞ undisturbed free-stream conditions

IV. INTRODUCTION

In analyzing the supersonic flow past a blunt body, different approaches are used for the different regions which, generally, are a subsonic region between the detached shock wave and that part of the body in the vicinity of the stagnation point, the supersonic region downstream of the subsonic region, and the mixed subsonic-supersonic region between the previous two. In the analysis of the entire problem many difficulties arise due to the relatively ill defined boundaries of these three regions of flow.

The calculation of the flow field between the bow shock wave and a blunt-nosed body traveling at supersonic or hypersonic speeds is of considerable interest, both from a mathematical and a physical point of view. On the mathematical side, it involves all three types of second-order partial differential equations - hyperbolic, parabolic, and elliptic - and includes the analytic and numerical difficulties associated with each type. On the physical side, the flow field properties are necessary for the analysis and design of space vehicles, which have become increasingly important due to the fast development in the aerospace industry.

In the supersonic region, the method of characteristics gives very complete and good results as long as the characteristic network is sufficiently refined; also, flow field properties must be known along some initial, noncharacteristic line in the supersonic region. With regard to the region of mixed subsonic-supersonic flow, a survey of the existing literature[1,2,6-16] gives, in general, two methods of approach to this type of problem. Method one is the so-called inverse method, which starts from an assumed shock shape to determine a body shape and integrates the equations of motion from the shock to body. Method two is the direct method, which proceeds from body to shock. Comparing these two different approaches, both of them give some satisfactory results. But from a practical and engineering point of view, the direct method is preferable. Both methods have a similar disadvantage in that an iteration scheme has to be used to determine, in the inverse method, the body shape and to determine the shock shape in the direct method. The advantage of the direct method over that of the inverse method lies mainly in the fact that the body shape is given and the shock shape is to be determined.

For both compressible and imcompressible flow, the momentum equations are non-linear, partly due to the fact that the bow shock wave gives rise to a rotational flow. This non-linearity makes numerical integration of the equations of motion for this type of problem almost a necessity.

The present paper describes a numerical method of the direct type which is used to analyze the region in the vicinity of the stagnation point by starting from the stagnation streamline. Different from the inverse method, the method of integral relations and from other previous direct methods, this method offers another possible technique for dealing with the subsonic region. The distribution of flow properties along the stagnation streamline in front of the body is required for this investigation. DeJarnette[3], using a finite-difference scheme developed by Lax[4], has applied this numerical method to the case of a wedge in supersonic flow with good results. In the present thesis a similar treatment is applied along the stagnation streamline for further investigation. First attempts to solve the whole subsonic region failed because of instabilities of the flow properties on the body. Because the numerical procedure is unstable, especially in the vicinity of the stagnation point, the inevitable small errors grow geometrically as the solution proceeds from the body to the shock[10,11]. This difficulty in calculation makes necessary further analysis and investigation in the vicinity of the stagnation point. Instead of solving the flow properties in the whole subsonic region, all work is concentrated in this analysis on that special portion of the flow field near the stagnation point which causes the most serious unstable phenomena. The present work may be considered as a first step toward investigating the eventual calculation of flow about a whole configuration. Further development to extend this analysis to a larger portion of the subsonic region has not been achieved here. However, this thesis explores a possible technique for handling this type of problem by a new approach.

This investigation requires in addition to freestream conditions, the shock stand-off distance and the distribution of the flow properties along the stagnation streamline. Several assumptions, such as steady, compressible, inviscid, and two-dimensional flow, are made in the analysis in order to render the governing equations amenable to numerical solution. Results of this investigation have been carefully examined and compared with those available from the analytic approach and experimental data[13,14]. However, due to the absence of certain exact results in the literature, some of the results of the present study are left uncompared. For a complete investigation it would be necessary to make up this deficit.

V. ANALYSIS

1. Basic Equations.

The governing equations for the steady, inviscid, compressible flow for the perfect gas to be investigated can be written[1,2]

$$\mathrm{div}\ (\rho\vec{V}) = 0 \tag{1}$$

$$\rho(\vec{V} \cdot \mathrm{grad})\ \vec{V} + \mathrm{grad}\ P = 0 \tag{2}$$

$$\vec{V} \cdot \mathrm{grad}\ \left(\frac{P}{\rho^{\gamma}} \right) = 0 \quad . \tag{3}$$

The finite-difference scheme employed in reference 3 will be used to solve the system (1) through (3) within only a limited portion of the shock-layer flow field generated by a circular cylinder in a supersonic freestream. In this two-dimensional case, and utilizing the body-oriented coordinate system of reference 3 (see Fig. 1), it has been shown in reference 3 that the nondimensionalized divergence form of the governing equations can be written

$$\frac{\partial a_m}{\partial x} + \frac{\partial b_m}{\partial y} + d_m = 0 \tag{4}$$

$$(m = 1,\ 2,\ 3\ ) \quad ,$$

where

$$\begin{aligned} a_1 &= \bar{\rho}\ \bar{u} & b_1 &= \bar{\rho}\ \bar{v}\ \lambda_x & d_1 &= 0 \\ a_2 &= \bar{P} + \bar{\rho}\bar{u}^2 & b_2 &= b_1\ \bar{u} & d_2 &= \bar{K}\ a_3 \\ a_3 &= a_1\ \bar{v} & b_3 &= (\bar{P} + \bar{\rho}\bar{v}^2)\lambda_x & d_3 &= -\ \bar{K}\ a_2 \quad , \end{aligned} \tag{5}$$

with the scale factor λ_x given by

$$\lambda_x = 1 + \bar{K}\,\bar{y} \,, \tag{6}$$

where $\bar{K}$ is the nondimensionalized local body curvature

$$\bar{K} = - \frac{d\theta}{d\bar{x}} \,. \tag{7}$$

For the circular cylinder to be studied in this work

$$\bar{K} = - \frac{L}{R} \,, \tag{8}$$

where R is the radius of the cylinder and L is an arbitrary non-dimensionalizing length.

Selecting

$$L = R \,, \tag{9}$$

Eq. (8) reduces to

$$\bar{K} = 1, \tag{10}$$

which allows the scale factor λ_x of Eq. (6) to be written

$$\lambda_x = 1 + \bar{y} \,. \tag{11}$$

2. Difference Equation for Non-Body Points.

Again as developed in reference 3, using the scheme suggested by Lax (reference 4), the finite-difference representation of Eq. (4) for points in the flow field not on the body can be expressed as

$$(a_m)_{k+1,\ell} = \frac{1}{2}\left[(a_m)_{k,\ell+1} + (a_m)_{k,\ell-1}\right] - \frac{\Delta x}{2\Delta y}\left[(b_m)_{k,\ell+1} - (b_m)_{k,\ell-1}\right] - \frac{\Delta x}{2}\left[(d_m)_{k,\ell+1} + (d_m)_{k,\ell-1}\right] \tag{12}$$

with $m = 1, 2, 3$,

where the subscripts k and ℓ refer to the order of mesh spacing (see Fig. 2) in the x and y directions respectively.

In the present analysis only four points in the flow field are to be considered, namely, the points (1,1), (1,3), (2,2) and (3,1), as shown in Fig. 2. Note that point (1,1) is taken as the stagnation point on the body, whereas point (3,1) will be the first body point that can be determined through the use of the other three points (1,1), (1,3) and (2,2). Note also that point (1,3) is the first point (nearest the body stagnation point) along the stagnation streamline at which initial data must be supplied in order to determine flow properties at intermediate point (2,2) and subsequently to calculate properties at point (3.1). In this restricted region of the flow field, in the near vicinity of and including the body stagnation point (1,1), the $\bar{y}$-coordinate in Eq. (11) will take on its maximum value of $2\Delta\bar{y}$ at the point (1,3). Also, since the cylinder radius R is considered large compared to the physical mesh spacing Δy, and in view of Eq. (9), there will be introduced the assumption

$$\Delta\bar{y} << 1 \; . \tag{13}$$

This leads to the Eq. (11) approximation

$$\lambda_x \cong 1 \; . \tag{14}$$

Assumption (13) will be applied at all four points in the present analysis because of the simplifications introduced in Eqs. (5) and for convenience of computation. When point (1,3) is moved upstream to the normal shock point, assumption (13) no longer holds. In this case,

λ_x will be greater than one, and the present analysis would then have to proceed without the approximation (14).

Substitution of Eqs. (10) and (14) allows the quantities a_1 through d_3 in Eqs. (5) to be written

$$\begin{array}{lll} a_1 = \bar{\rho}\,\bar{u} & b_1 = \bar{\rho}\,\bar{v} & d_1 = 0 \\ a_2 = \bar{P} + \bar{\rho}\bar{u}^2 & b_2 = b_1\,\bar{u} & d_2 = a_3 \\ a_3 = a_1\bar{v} & b_3 = \bar{P} + \bar{\rho}\bar{v}^2 & d_3 = -\,a_2\ . \end{array} \tag{15}$$

3. <u>Properties at Intermediate Point (2,2)</u>.

For determination of flow properties at point (2,2) the difference equation (12) becomes

$$a_{m22} = \frac{1}{2}\,(a_{m13} + a_{m11}\,) - \frac{\Delta\bar{x}}{2\Delta\bar{y}}\,(b_{m13} - b_{m11}) - \frac{\Delta\bar{x}}{2}\,(d_{m13} + d_{m11})$$

$$m = (1,\ 2,\ 3)\ , \tag{16}$$

where the subscripts on a_m, b_m, and d_m refer to one of the particular mesh points (2,2), (1,3), or (1,1) shown in Fig. 2. In accordance with Eqs. (15), the properties at points (1,1) and (1,3) will be

$$\begin{array}{lll} a_{111} = 0 & b_{111} = 0 & d_{111} = 0 \\ a_{211} = \bar{P}_{11} = \bar{P}_{stag} & b_{211} = 0 & d_{211} = 0 \\ a_{311} = 0 & b_{311} = a_{211} & d_{311} = -\,a_{211} \end{array} \tag{17}$$

and

$$
\begin{array}{lll}
a_{113} = 0 & b_{113} = \bar{\rho}_{13}\,\bar{v}_{13} & d_{113} = 0 \\
a_{213} = \bar{P}_{13} & b_{213} = 0 & d_{213} = 0 \\
a_{313} = 0 & b_{313} = \bar{P}_{13} + \bar{\rho}_{13}\,\bar{v}_{13}^{\,2} & d_{313} = -\bar{P}_{13}
\end{array}
\tag{18}
$$

Substitution of these values into Eq. (16) with m = 1, 2, 3 yields the following three expressions:

$$a_{122} = -\frac{\Delta\bar{x}}{2\Delta\bar{y}}\,\bar{\rho}_{13}\,\bar{v}_{13} \tag{19}$$

$$a_{222} = \frac{1}{2}\,(\bar{P}_{13} + \bar{P}_{11}) \tag{20}$$

$$a_{322} \cong \frac{\Delta\bar{x}}{2\Delta\bar{y}}\,(\bar{P}_{11} - \bar{P}_{13} - \bar{\rho}_{13}\,\bar{v}_{13}^{\,2}) \quad , \tag{21}$$

where the assumption of (13) has again been applied in developing Eq. (21).

With a known value of the freestream Mach number M_∞, the stagnation point pressure, $\bar{P}_{stag}$, can be determined from the relation[5]

$$\bar{P}_{stag} = \frac{P_{stag}}{\rho_\infty V_\infty^{\,2}} = \frac{1}{\gamma M_\infty^{\,2}}\left[\frac{(\gamma+1)\,M_\infty^{\,2}}{2}\right]^{\frac{\gamma}{\gamma-1}}\left[\frac{\gamma+1}{2\gamma\,M_\infty^{\,2} - (\gamma-1)}\right]^{\frac{\gamma}{\gamma-1}} \tag{22}$$

Also, the Bernoulli Equation can be applied along the stagnation streamline to obtain the relationships

$$\frac{\bar{\rho}_{13}\bar{v}_{13}^{\,2}}{\bar{P}_{13}} = \frac{2\gamma}{\gamma-1}\left[\left(\frac{\bar{P}_{stag}}{\bar{P}_{13}}\right)^{\frac{\gamma-1}{\gamma}} - 1\right] \tag{23}$$

and

$$\bar{v}_{13} = -\sqrt{\frac{2\gamma}{\gamma-1}\left(\frac{\bar{P}_{stag}}{\bar{\rho}_{stag}}\right)\left[1-\left(\frac{\bar{P}_{13}}{\bar{P}_{stag}}\right)^{\frac{\gamma-1}{\gamma}}\right]}\ , \tag{24}$$

where the ratio $\bar{P}_{stag}/\bar{\rho}_{stag}$ can be expressed as the following function of freestream Mach Number:

$$\frac{\bar{P}_{stag}}{\bar{\rho}_{stag}} = \frac{\gamma-1}{2\gamma}\left[1+\frac{2}{(\gamma-1)\,M_\infty^{\ 2}}\right]. \tag{25}$$

Therefore, introducing the definitions

$$\xi = \frac{\bar{P}_{stag}}{\bar{P}_{13}} \tag{26}$$

$$\sigma = \frac{\bar{\rho}_{13}\bar{v}_{13}^{\ 2}}{\bar{P}_{13}} = \frac{2\gamma}{\gamma-1}\left(\xi^{\frac{\gamma-1}{\gamma}} - 1\right) \tag{27}$$

and

$$\tau = \frac{\Delta\bar{y}}{\Delta\bar{x}}\ , \tag{28}$$

Equations (19) through (21) can be written

$$a_{122} = -\frac{\sigma\,\bar{P}_{stag}}{2\tau\xi\,\bar{v}_{13}} \tag{29}$$

$$a_{222} = \frac{\bar{P}_{stag}}{2\xi}(1+\xi) \tag{30}$$

and

$$a_{322} \cong -\frac{\bar{P}_{stag}\,(\sigma+1-\xi)}{2\tau\xi}\ . \tag{31}$$

As seen from Eqs. (15), the above relations can be used to determine the y-component of velocity, $\bar{v}_{22}$, at intermediate point (2,2) as

$$\bar{v}_{22} = \frac{a_{322}}{a_{122}} = \bar{v}_{13} \left(1 - \frac{\xi - 1}{\sigma}\right) , \tag{32}$$

where $\bar{v}_{13}$ can be expressed in terms of ξ and M_∞ by combining Eqs. (24) and (25) to yield

$$\bar{v}_{13} = - \bar{V}_m \sqrt{1 - \xi^{-\frac{\gamma-1}{\gamma}}} \quad . \tag{33}$$

The term $\bar{V}_m$ in (33) is the maximum speed constant given by[5]

$$\bar{V}_m = \left[1 + \frac{2}{(\gamma-1) M_\infty^{\;2}}\right]^{\frac{1}{2}} \quad . \tag{34}$$

Combining Eqs. (32) and (33), the ratio $\bar{v}_{22}/\bar{V}_m$ can be expressed

$$\frac{\bar{v}_{22}}{\bar{V}_m} = - \left(1 - \frac{\xi-1}{\sigma}\right) \left[1 - \frac{1}{\xi^{\frac{\gamma-1}{\gamma}}}\right]^{\frac{1}{2}} , \tag{35}$$

which is seen to be a function of only the pressure ratio ξ. A plot of the ratio $\bar{v}_{22}/\bar{V}_m$ from Eq. (35), with $\gamma = 1.4$, is shown in Figure 3. Note that an ξ value greater than 5.23 need not be considered since $\bar{v}_{22}$ becomes positive beyond this point and would correspond to the physically unrealistic case of reverse flow at point (2,2). The fact that this occurs in Eq. (32), however, is due entirely to the numerical difference scheme used in the analysis and has no physical implications.

To find the $\bar{u}$-component of velocity at any point in the flow field consider the identity

$$\frac{a_2}{a_1} = \frac{\bar{P}}{\bar{\rho}\,\bar{u}} + \bar{u}$$

or, rearranging,

$$\bar{u}^2 - \frac{a_2}{a_1}\bar{u} + \frac{\bar{P}}{\bar{\rho}} = 0 \quad , \tag{36}$$

which follows directly from the definitions (5).

The $\bar{P}/\bar{\rho}$ ratio in Eq. (36) can be determined from Bernoulli's equation as

$$\frac{\bar{P}}{\bar{\rho}} = \frac{\gamma - 1}{2\gamma} (\bar{V}_m^{\,2} - \bar{u}^2 - \bar{v}^2) \quad . \tag{37}$$

Substitition of Eq. (37) into (36) and solving for $\bar{u}$ produces the results

$$\bar{u} = \frac{\gamma}{\gamma + 1} \left(\frac{a_2}{a_1} \right) \left\{ 1 \pm \sqrt{1 - \left(\frac{\gamma^2 - 1}{\gamma^2} \right) \left[\frac{\bar{V}_m^{\,2} - \bar{v}^2}{\left(\frac{a_2}{a_1} \right)^2} \right]} \right\} . \tag{38}$$

In order for values of $\bar{u}$ calculated from Eq. (38) to remain real, the grouping of terms shown under the radical must remain non-negative. Also, it can be seen that this grouping will have a value less than unity since $\bar{V}_m > \bar{v}$ at all points in the flow field. Thus, it is possible to obtain two real values for $\bar{u}$, depending upon which sign is selected in Eq. (38).

DeJarnette in Ref. 3 has shown that the positive sign in Eq. (38) is associated with a supersonic field, so in the present blunt-body analysis (where the shock-layer flow is subsonic) the negative sign should be used. The boundary restriction which arises from the requirement that $\bar{u}$ remain real in Eq. (38) can be expressed

$$\left(\frac{a_2}{a_1} \right)^2 \geqq \frac{\gamma^2 - 1}{\gamma^2} \left(\bar{V}_m^{\,2} - \bar{v}^2 \right) \quad . \tag{39}$$

The main purpose of the present analysis is to find out a possible way to solve for the flow properties at points (2,2) and (3,1) in terms of M_∞, τ and ξ. Among these three parameters, Mach number, M_∞, of a supersonic flow is an independent variable. τ and ξ involve the dependent variables $\Delta\bar{x}$, $\Delta\bar{y}$, and $\bar{P}_{13}$ ($\bar{P}_{11}$ is a fixed value for a certain M_∞ supersonic flow), which are related to one another. For different $\Delta\bar{y}$ values $\bar{P}_{13}$ must have different corresponding values due streamline inside the shock layer. Also, as will be shown, $\Delta\bar{x}$ varies with respect to $\Delta\bar{y}$. This leads to the fact that τ and ξ play an important role in the present investigation. By using a finite difference scheme step-by-step from an initial starting line (in the present case it is the stagnation streamline), this approach developes several restrictions and limitations on the values of τ and ξ by the nature of the flow condition and properties at the intermediate point (2,2) and at the body point (3,1). This development can be set in the following order:

(a) By the requirement that $\bar{v}$ remain negative at point (2,2), a restriction is formed for τ and ξ values (see Fig. 3).

(b) By limiting the value of ξ to its maximum normal-shock value on the stagnation streamline inside the subsonic shock layer a restraint on ξ is obtained.

(c) By limiting the total velocity at point (2,2), noting that V_{22} must remain less than its sonic value, another restriction on τ and ξ values is obtained.

(d) By the requirement that conditions along the stagnation streamline are restrained by the pressure distribution along that line, which is a function of freestream Mach number only, a more restricted condition on τ and ξ values must be considered in the present problem. Values of τ and ξ can be used as preliminary parameters in obtaining the $\Delta\bar{y}$, $\Delta\bar{x}$ and $\bar{P}_{13}$ values for solution of the pertinent equations.

The following sections contribute to the investigation of these developments in more detail.

4. <u>First τ-ξ Boundary Curve</u>.

At point (2,2) the ratio a_{222}/a_{122}, shown on the left of inequality (39), is determined from Eqs. (29) and (30) as the following function of ξ and τ:

$$\frac{a_{222}}{a_{122}} = -\frac{\tau(1+\xi)}{\sigma}\,\bar{v}_{13} \quad . \tag{40}$$

Combining Eqs. (40) and (33), with use of (27), the ratio a_{222}/a_{122} in Eq. (40) can be expressed

$$\frac{a_{222}}{a_{122}} = \frac{\frac{\gamma-1}{2\gamma}(\xi+1)\,\tau\,\bar{V}_m}{\sqrt{\xi^{\frac{\gamma-1}{\gamma}}(\xi^{\frac{\gamma-1}{\gamma}} - 1)}} \quad . \tag{41}$$

At fixed M_∞, the right side of inequality (39) involves only ξ when evaluated at point (2,2), as can be seen from the expression for $\bar{v}_{22}$ in Eq. (35). Substituting (35) and (41) into (39), the boundary restriction determined for properties at point (2,2) yields the following restraint on selected values of ξ and τ:

$$\tau \geq \frac{2}{\xi+1}\sqrt{\frac{\gamma+1}{\gamma-1}\left[\xi^{\frac{\gamma-1}{\gamma}}(\xi^{\frac{\gamma-1}{\gamma}} - 1) - \left(\frac{\gamma+1}{2\gamma}\right)^2(\sigma + 1 - \xi)^2\right]} \quad . \tag{42}$$

A plot of this τ-ξ boundary for the equality condition in Eq. (42) is shown in Fig. 4. It is interesting to note that this boundary is independent of free stream Mach number, M_∞, and is double-valued in ξ between τ values of 0.7756714 and 0.8667776. Note that for any ξ-value within the range

$$1 \leq \xi \leq 5.23 \quad , \tag{43}$$

the corresponding value selected for τ must exceed that given by the curve in Fig. 4.

5. <u>Body Point Equations</u>.

Before proceeding further with the calculation of other flow properties at the intermediate point (2,2), it will prove beneficial to develop relationships for predicting body-point properties at (3,1). Whereas a symmetrical mesh scheme, e.g.

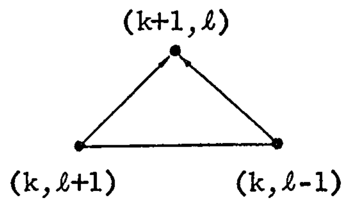

was used for non-body points $(k+1,\ell)$, dependent upon properties at $(k,\ell+1)$ and $(k,\ell-1)$, the body-point determination will utilize an asymmetric mesh step,

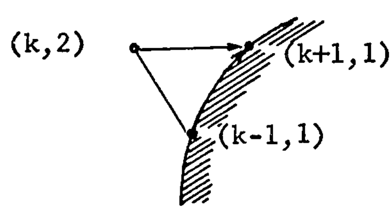

giving results at (k+1,1) in terms of properties at the proceeding body point (k-1,1) and the closest intermediate point (k,2). This again is the scheme used in Ref. 3, and the corresponding difference equation developed in that reference for prediction of body-point properties is

$$(a_m + \Delta\bar{x}\ d_m)_{k+1,1} = (a_m - \Delta\bar{x}\ d_m)_{k-1,1}$$

$$- \frac{2\Delta\bar{x}}{\Delta\bar{y}} \left\{ (b_m)_{k,2} - \frac{1}{2} \left[(b_m)_{k+1,1} + (b_m)_{k-1,1} \right] \right\}$$

$$(m = 1,\ 2,\ 3) \quad . \tag{44}$$

Specializing this equation to the present two-dimensional case so that Eqs. (15) apply, and noting that the $\bar{v}$-component of velocity vanishes on the body, Eq. (44) yields the following three relationships at the body point (3,1):

$$a_{131} = - \frac{2b_{122}}{\tau} \tag{45}$$

$$a_{231} = \bar{P}_{stag} - \frac{2b_{222}}{\tau} \tag{46}$$

$$\Delta\bar{y} = \frac{2b_{322} - (\bar{P}_{31} + \bar{P}_{stag})}{a_{231} + \bar{P}_{stag}} \tag{47}$$

The interrelationship that must exist between selected values of ξ, $\Delta\bar{y}$, and $\Delta\bar{x}$ will now be demonstrated using the total equational system (29) through (31) coupled with (45) through (47). Utilizing Eqs. (29) through (31), it can be seen that only the two parameters ξ and τ need be specified in order to calculate a_{122}, a_{222}, a_{322}, form appropriate ratios, such as Eq. (32), and thus determine all flow properties $\bar{v}_{22}$, $\bar{u}_{22}$, $\bar{P}_{22}$, and $\bar{\rho}_{22}$ at the intermediate point (2,2).

Hence, from Eqs. (45) and (46), where

$$b_{122} \equiv \bar{\rho}_{22}\,\bar{v}_{22} \tag{48}$$

and

$$b_{222} \equiv b_{122}\,\bar{u}_{22} \quad , \tag{49}$$

the quantities a_{131} and a_{231} can be determined as functions of ξ and τ only. Having these two values, note that the body-point velocity, $\bar{u}_{31}$, can be found as one root of the quadratic solution (38), namely,

$$\bar{u}_{31} = \frac{\gamma}{\gamma+1}\left(\frac{a_{231}}{a_{131}}\right)\left\{1 - \sqrt{1 - \left(\frac{\gamma^2-1}{\gamma^2}\right)\left(\frac{a_{131}}{a_{231}}\,\bar{V}_m\right)^2}\right\}. \tag{50}$$

The body-point pressure, $\bar{P}_{31}$, can now be calculated from the relation (see Eqs. (5))

$$\bar{P}_{31} = a_{231} - a_{131}\,\bar{u}_{31} \quad .$$

Thus, all quantities on the right side of Eq. (47) are known, and thus the $\Delta\bar{y}$ value can be calculated. Since, however, τ had to be specified, the determination of $\Delta\bar{y}$ also determines a unique value for $\Delta\bar{x}$. So it appears that arbitrary selection of any <u>two</u> of the three quantities ξ, $\Delta\bar{y}$, and $\Delta\bar{x}$ automatically fixes the third quantity through the equational relationships which have been developed.

6. Mesh Spacing Relationships.

Using an IBM 7040 digital computer, $\Delta\bar{x}$ and $\Delta\bar{y}$ values were computed at various constant values of ξ, and these calculations were repeated over a range of freestream Mach numbers, M_∞. A typical plot of $\Delta\bar{x}$ versus $\Delta\bar{y}$, with ξ treated parametrically, is shown in Fig. 5. Note the boundary AB, which reflects the calculational restriction given in Eq. (42). For each M_∞ there exists a minimum value of $\Delta\bar{x}_{min}$ below which no real solutions to the equational system (29) through (31) and (45) through (47) can be found. In fact, no real solutions exist throughout the region I, outside the boundary AB. Also, note the asymptotically increasing behavior of $\Delta\bar{x}$ along AB at very small values of $\Delta\bar{y}$. This is an unfortunate circumstance of the present finite-difference scheme. It was hoped that as the point (1,3) was moved closer to the stagnation point (1,1), the corresponding body point (3,1) would also approach (1,1). However, the present results indicate that, after having reached a certain point of closest approach, $\Delta\bar{x}_{min}$, the first body point (3,1) moves rapidly away in the opposite direction as the mesh spacing, $\Delta\bar{y}$, is further decreased.

These principal numerical results of the present study can be modified slightly by certain physical considerations, which will now be discussed, but the detrimental trends already noted in the behavior of $\Delta\bar{x}$ continue to persist.

7. Physical Restrictions.

Corresponding to any M_∞, an upper limit on ξ can be determined by considering the point (1,3) to be moved all the way to the immediate downstream face of the bow shock wave, which at this point will be normal to the freestream flow direction. There then results the limiting value

$$\xi_{max} = \left[\frac{(\gamma + 1)^2 M_\infty^{\ 2}}{4\gamma M_\infty^2 - 2\ (\gamma - 1)} \right]^{\frac{\gamma}{\gamma-1}} . \tag{51}$$

This constitutes the oblique boundary CD shown in Fig. 5. For all $M_\infty \geq 1$, values of ξ_{max} from Eq. (51) will be less than the ξ=5.23 value determined from Eq. (35) at $\bar{v}_{22} = 0$ and $\gamma = 1.4$. On the other hand, if point (1,3) is moved across the shock into the freestream, ξ will far exceed the limit shown in Fig. 4.

Another physical restriction not yet considered involves the total velocity, $\bar{V}_{22}$, at intermediate point (2,2). It will be noted that the limit curve in Fig. 4 corresponds to the root

$$\bar{u}_{22} = \frac{\gamma}{\gamma + 1}\ \frac{a_{222}}{a_{122}} \tag{52}$$

of Eq. (38), where the ratio a_{222}/a_{122} in (52) is obtained from (39) as

$$\frac{a_{222}}{a_{122}} = \frac{\gamma^2-1}{\gamma^2}\ (\bar{V}_m^{\ 2} - \bar{v}_{22}^{\ 2}) . \tag{53}$$

Hence, at this condition, $\bar{V}_{22}$ becomes

$$\bar{V}_{22} = \sqrt{\bar{u}_{22}^{\,2} + \bar{v}_{22}^{\,2}} = \left(\bar{V}_m\sqrt{\frac{\gamma - 1}{\gamma + 1}}\right)\sqrt{1 + \frac{2}{\gamma - 1}\left(\frac{\bar{v}_{22}}{\bar{V}_m}\right)^2}\,. \tag{54}$$

Since the coefficient of the radical in this expression is the sonic speed at any point in the flow, it is apparent that $\bar{V}_{22}$ will be supersonic along the boundary given by the equality in Eq. (42). Since the shock-layer flow being studied is subsonic, a new restriction must be established corresponding to

$$\bar{V}_{22} \leqq \bar{V}_m \sqrt{\frac{\gamma - 1}{\gamma + 1}}\ . \tag{55}$$

The value of $\bar{V}_{22}$ can be reduced to that of the equality in Eq. (55) by reducing the limit value of the $\bar{u}$-component slightly below that given by (52). The corresponding τ-ξ limit line relation is determined by first noting that the substitution

$$\bar{u}_{22} = \sqrt{\left(\frac{\gamma - 1}{\gamma + 1}\right)\bar{V}_m^{\,2} - \bar{v}_{22}^{\,2}} \tag{56}$$

in Eq. (38) yields

$$\frac{a_{222}}{a_{122}} = \frac{\left(\frac{\gamma - 1}{\gamma}\right)\bar{V}_m^{\,2} - \bar{v}_{22}^{\,2}}{\sqrt{\left(\frac{\gamma - 1}{\gamma + 1}\right)\bar{V}_m^{\,2} - \bar{v}_{22}^{\,2}}}\,. \tag{57}$$

This value of the ratio a_{222}/a_{122} is seen to be somewhat greater than that given by the equality sign in Eq. (39). Substituting (35) and (41) into Eq. (57), the new τ-ξ boundary replacing relationship (42) becomes

$$\tau \geqq \frac{2}{\xi+1}\left(\frac{\gamma}{\gamma-1}\right)\frac{\sqrt{\xi^{\frac{\gamma-1}{\gamma}}\left(\xi^{\frac{\gamma-1}{\gamma}}-1\right)\left[\frac{\gamma-1}{\gamma}-\left(1-\frac{\xi-1}{\gamma}\right)^{2}\left(1-\frac{1}{\xi^{\frac{\gamma-1}{\gamma}}}\right)\right]}}{\sqrt{\frac{\gamma-1}{\gamma+1}-\left(1-\frac{\xi-1}{\sigma}\right)^{2}\left(1-\frac{1}{\xi^{\frac{\gamma-1}{\gamma}}}\right)}} \quad (58)$$

Denoting the value of τ corresponding to the equality in (58) by τ^*, such that

$$\tau = \tau^* \quad \text{at} \quad \bar{V}_{22} = \bar{V}_m \sqrt{\frac{\gamma - 1}{\gamma + 1}} \ (\text{i.e. at } M_{22} = 1) \ , \qquad (59)$$

and using τ_{min} for the equality τ in (42), the ratio τ^*/τ_{min} can be written as

$$\frac{\tau^*}{\tau_{min}} = \frac{\left[\frac{\gamma-1}{\gamma}\bar{V}_m^{\,2} - \bar{v}_{22}^{\,2}\right]\sqrt{\frac{\gamma-1}{\gamma+1}\left(\bar{V}_m^{\,2} - \bar{v}_{22}^{\,2}\right)}}{\frac{\gamma-1}{\gamma}\left(\bar{V}_m^{\,2} - \bar{v}_{22}^{\,2}\right)\sqrt{\frac{\gamma-1}{\gamma+1}\bar{V}_m^{\,2} - \bar{v}_{22}^{\,2}}} \ . \qquad (60)$$

At fixed values of ξ, within the range given in (43), Eq. (60) shows that τ^* will be only slightly greater than τ_{min}. In Fig. 4 the difference between the two curves is essentially inperceptable. The final $\Delta\bar{x}$-$\Delta\bar{y}$ plots (Figs. 8 through 15) include the condition (58) rather than (42), although the boundary difference is quite small as previously indicated.

A final physical restriction which must be considered is the interdependence between ξ and $\Delta\bar{y}$. The pressure gradient along the stagnation streamline is determined by freestream conditions and body geometry. Hence, a particular value of ξ at point (1,3) requires that the point have a particular location in terms of $\Delta\bar{y}$. Upon investigating the ξ distribution along the stagnation streamline, the important information required to be known is the shock standoff distance, δ, and the relationship between ξ and y-displacement distance along the stagnation streamline.

First, as far as the shock stand-off distance is concerned, most of the literature [1,2,6-12] only gives information about axisymmetrical bodies. However, Fuller[13] and Hamaker[14] give exact solutions for a supersonic flow past a circular cylinder. With this information, the shock stand-off distance can be used as a reference in further investigation about the ξ-distribution along the stagnation streamline. In the present analysis, when δ is nondimensionalized in terms of the cylinder radius R, it becomes simply the maximum value of y measured along the stagnation streamline. Hence, noting that the y distance to point (1,3) is $2\Delta\bar{y}$, placement of the point (1,3) at its limiting position immediately at the normal-shock gives the maximum value of $\Delta\bar{y}$ as

$$(\Delta\bar{y})_{max} = \frac{y_{max}}{2} = \frac{\delta}{2R} . \tag{61}$$

Using stand-off distances given by Fuller in Ref. 13, values of $(\Delta\bar{y})_{max}$ are shown as a function of freestream Mach number in Fig. 6. This limitation will also appear in the $\Delta\bar{x}$ - $\Delta\bar{y}$ plots, similar to Fig. 5, as a vertical limit line on $\Delta\bar{y}$. Any value of $\Delta\bar{y}$ greater than the $(\Delta\bar{y})_{max}$ given in (61) will cause the point (1,3) to fall outside the subsonic shock layer into the freestream flow, a condition which already has been discarded in previous analysis (see Eq. (51)).

Now a relationship for the stagnation line ξ-distribution must be obtained in order to represent this third physical restriction as a line of restraint on the final $\Delta\bar{x}$ - $\Delta\bar{y}$ plots, Figs. 8 through 15. A survey of the existing literature(6-12) yields no information about the pressure distribution along the stagnation streamline inside the shock layer for the case of the two-dimensional cylinder. All approaches are restricted to the flow properties on the shock and body surface, sonic line location, and some special points in the flow fields. Therefore, an approximate analytic method to determine this relationship will be employed here using the potential flow solution

$$\Phi_{\text{at } \omega=o} = A_1 r \left[1 + \left(\frac{R}{r} \right)^2 \right], \tag{62}$$

where the coefficient A_1 is a function of freestream conditions only and is given by

$$A_1 = - \left[\frac{\left(\frac{b}{R} \right)^2}{\left(\frac{b}{R} \right)^2 - 1} \right] \left| V_{N.S.} \right| \quad . \tag{63}$$

The significant quantities r, b, and $V_{N.S.}$ are shown in Fig. 7. The solution (62) was introduced by Truitt[15]; however, its development from a more general potential flow solution can be obtained following treatments analysis to those presented by Tseng[16] and by Hildebrand[17] in the axisymmetric case.

The velocity at point (1,3) can now be obtained by applying the potential flow relation[16]

$$v = \frac{\partial \Phi}{\partial r} \quad . \tag{64}$$

Differentiating Eq. (62) in accordance with (64), and nondimensionalizing the resulting velocity in terms of the freestream value, there is obtained the following expression for $\bar{v}_{13}$:

$$\bar{v}_{13} = - \left[\frac{(b/R)^2}{(b/R)^2 - 1} \right] \left[1 - \left(\frac{R}{r} \right)^2 \right] \left[\frac{(\gamma-1)\, M_\infty^{\,2} + 2}{(\gamma+1)\, M_\infty^{\,2}} \right] \tag{65}$$

It should be noted that this potential flow solution to the blunt-body problem assumes the bow shock wave to be concentric with the body, at least at the shock vortex ($\omega=0$, $r = b$). Thus, in terms of shock stand-off distance, δ, the b/R-ratio in (65) can be expressed

$$\frac{b}{R} = 1 + \frac{\delta}{R}$$

or, utilizing (61), in terms of $(\Delta\bar{y})_{max}$ this becomes

$$\frac{b}{R} = 1 + 2\ (\Delta\bar{y})_{max} \tag{66}$$

Therefore, Eq. (65) can be written

$$\bar{v}_{13} = - f(M_\infty) \left[1 - \left(\frac{R}{r} \right)^2 \right] , \tag{67}$$

where the freestream Mach number function $f(M_\infty)$ is given by

$$f(M_\infty) = \frac{\left[2+(\gamma-1)\ M_\infty^{\ 2}\right] \left[1 + 2(\Delta\bar{y})_{max}\right]^2}{4(\gamma+1)\ M_\infty^{\ 2}\ (\Delta\bar{y})_{max} \left[1 + (\Delta\bar{y})_{max}\right]} \tag{68}$$

with values of $(\Delta\bar{y})_{max}$ presented in Fig. 6.

In terms of locating the point (1,3), note that the variable distance, r, in Eq. (67) can be written

$$r = r_{13} = R + 2\ \Delta y$$

for this special case. Hence, (67) becomes

$$\bar{v}_{13} = - 4f\ (M_\infty)\ \frac{\Delta\bar{y}(1 + \Delta\bar{y})}{(1 + 2\Delta\bar{y})^2} \quad . \tag{69}$$

Applying Bernoulli's Equation (37) with $\bar{u} = 0$ at the point (1,3) and also using the energy relation, Eq. (3), along the stagnation streamline, the ξ value may be expressed as

$$\xi = \left(1 - \frac{\bar{v}_{13}^{\ 2}}{\bar{V}_m^{\ 2}}\right)^{-\frac{\gamma}{\gamma-1}} \tag{70}$$

Finally, the ξ distribution from the stagnation point to the normal shock point for a fixed M_∞ is obtained by substituting Eqs. (34) and (69) into (70) to give

$$\xi = \left\{ 1 - g(M_\infty) \left[\frac{\Delta\bar{y}(1 + \Delta\bar{y})}{(1 + 2\Delta\bar{y})^2} \right]^2 \right\}^{-\frac{\gamma}{\gamma-1}} \tag{71}$$

where $g(M_\infty)$ is a function of M_∞ only given by

$$g(M_\infty) = \frac{16(\gamma-1)\, M_\infty^{\ 2} f^2}{2 + (\gamma-1)\, M_\infty^{\ 2}} \tag{72}$$

Distributions represented by Eq. (71) are shown in each of the final $\Delta\bar{x}$ - $\Delta\bar{y}$ plots, Figs. 8 through 15.

VI. RESULTS AND DISCUSSION

Computations have been carried out by an IBM 7040 electronic digital computer to obtain variation of the parameters $\Delta\bar{x}$ and $\Delta\bar{y}$, and the ξ distribution along the stagnation streamline for various Mach numbers ranging from $2 \leq M_\infty \leq \infty$ for $\gamma = 1.4$, for the purpose of defining the limits on $\Delta\bar{x}$ and $\Delta\bar{y}$ shown in Fig. 16. In this calculation, τ is a preliminary parameter which is related to the choice of the mesh spacing in the x and y directions. The boundary curve CD arises from the fact that ξ has a limiting maximum value for a given M_∞ for the general case, since any increase above this value will cause the mesh point (1,3) to fall outside the shock layer. Curve DE is obtained directly from the distribution of ξ along the stagnation streamline inside the shock layer found by moving the point (1,3) upstream to the normal shock. As τ increases above τ^* the curve AB moves upward, so that the curve AB can be considered as a boundary curve excluding the region I from the present analysis. Area II is excluded by boundary curve CD. By Fuller's exact solution[13] for the shock stand-off distance for two dimensional supersonic flow past a circular cylinder, $(\Delta\bar{y})_{max}$ can be obtained from Eq. (61), which is shown on Fig. 16. Therefore, area III is also excluded from study in the present analysis. The region remaining for use in the calculation of the flow properties at points (2,2) and (3,1) is, therefore, the one bounded by curves AC, CD and the line $(\Delta\bar{y})_{max}$. In this region, curve DE is more significant than the others since it represents the analytic pressure distribution along the stagnation streamline inside the shock layer. On curve DE the point E represents the minimum value of $\Delta\bar{x}$. This value can be considered the most optimistic one for this parameter, for the assumed pressure distribution, to be used in solving the present problem. It is interesting to note here that the $\Delta\bar{y}$ value corresponding to the point E is relatively independent of M_∞. An examination of the $\Delta\bar{x}$ and $\Delta\bar{y}$ values for point E in the range of freestream Mach number from two to infinity, shows that the assumption (13) has not been voilated. This gives rise to the possibility of using this finite difference scheme in the solution of the general problem.

For the extreme case of point (1,3) located at the normal shock position, assumption (13) will no longer be valid since here Δy assumes a considerable value of λ_x becomes greater than unity. From Eq. (47) and those related equations which may be affected by $\lambda_x > 1$, for the points (2,2) and (1,3), it is found that the boundary curve AB in Fig. 16 will move upward.

Using the finite difference scheme developed here, with values of $\Delta\bar{x}$ and $\Delta\bar{y}$ restricted to the distribution lines ED, the values of the non-dimensionalized pressure, density, and local Mach number were calculated at the body point (3,1). The distribution of these properties along the body corresponds to a variation of the mesh size and hence to a change in the physical location of the point (3,1). These results are plotted in Figs. 17 and 18. A comparison shows poor agreement in actual numerical value. The trend of the variations, however, does agree with Fuller's exact results in reference 13.

Further investigation in more detail, coupled with some enlightened modifications to this analysis, might tend to improve these somewhat unfavorable results. Therefore, further application and generalization of the present technique are encouraged in order to achieve a new method of dealing with the problem which has been analyzed here.

VII. CONCLUSIONS

As the result of the present work, the following conclusions can be reached:

(1) This analysis, restricted to the vicinity of the stagnation point, has many restraints due to the physical limitations of the flow field properties. These results indicate that for a complete investigation many difficulties will arise in developing the more enlightened assumptions required to solve the general problem. Therefore, a full scale investigation should be carried out using more careful assumptions.

(2) Different distributions of the flow properties along the initial starting line will change the results of the present work considerably. Therefore, it is important to investigate this effect on solutions using different starting distributions found by either theoretical or experimental means.

(3) Variations in the flow properties calculated along the body surface using the present numerical method exhibit proper trends with change in location along the body. However, the actual magnitudes of these properties are not predicted correctly.

(4) The present thesis gives a starting point from which this type of problem may be made solvable. By applying more enlightened assumptions, a modification of the present method perhaps can be used to obtain more reasonable results.

VIII. ACKNOWLEDGMENTS

The author is especially grateful and deeply indebted to and for their guidance, patience and inspiration leading to the completion of this thesis.

The author also desires to express his thanks to for his enlightening instruction and concern during the author's study in Virginia Polytechnic Institute.

IX. BIBLIOGRAPHY

1. Van Dyke, M. D.: The Supersonic Blunt-Body Problem-Review and Extension. J. Aero/Space Sci., Vol. 25, No. 8, pp. 485-496, Aug. 1958.

2. Van Dyke, M. D. and Gordon, H. D.: Supersonic Flow Past a Family of Blunt Axisymmetric Bodies. NASA TR R-1, 1959.

3. DeJarnette, F. R.: Numerical Solution of Inviscid Hypersonic Flows for Nonequilibrium Vibration and Dissociation Using an "Artificial Viscosity" Method. Ph.D. Thesis, VPI., March 1965.

4. Lax, P. D.: Weak Solution of Nonlinear Hypersonic Equations and their Numerical Computation. Commun. Pure Appl. Math., Vol. VII, pp. 159-193, 1954.

5. Ames Research Staffs: Equations, Tables, and Charts for Compressible Flow. NACA Report 1135, 1953.

6. Belotserkovskii, O. M.: Flow with a Detached Shock Wave about a Symmetric Profile. Appl. Math. and Mech., Vol. 22, No. 2, pp. 279-296, 1958.

7. Belotserkovsky, O. M.: Flow Past a Circular Cylinder with a Detached Shock Wave. Doklady Akademia Nauk SSSR. Vol. 113, No. 3, pp. 509-512, 1957.

8. Garabedian, P. R., and Lieberstein, H. M.: On the Numerical Calculation of Detached Bow Shock Wave in Hypersonic Flow. J. Aeronaut. Sci., Vol. 25, No. 2, pp. 109-118, Feb. 1958.

9. Hida, K.: An Approximate Study on the Detached Shock Wave in Front of a Circular Cylinder and a Sphere. J. Phys. Soci. of Japan. Vol. 8, No. 6, pp. 740-745, Dec. 1953.

10. Penland, J. A.: Aerodynamic Characteristics of a Circular Cylinder at Mach Number 6.86 and Angle of Attack up to 90°. NACA TN 3861, 1957.

11. Valio-Laurin, R. and Ferri, A.: Theoretical Investigation of the Flow Field about Blunt-Nosed Bodies in Supersonic Flight. J. Aero/Space Sci., Vol. 25, No. 12, pp. 761-770, Dec. 1958.

12. Hayes, W. D., and Probstein, R. F.: Hypersonic Flow Theory. Academic Press, New York, 1959.

13. Fuller, F. B.: Numerical Solutions for Supersonic Flow of an Ideal Gas around Blunt Two-Dimensional Bodies. NASA TN D-791, July 1961.

14. Hamaker, F. M.: Numerical Solution of the Flow of a Perfect Gas over a Circular Cylinder at Infinite Mach Number. NASA MEMO 2-25-59A, March 1959.

15. Truitt, R. W.: Hypersonic Aerodynamics. The Ronald Press Co., New York, 1959.

16. Tseng, W. Y.: Potential Flow Solution of the Supersonic Blunt-Body Problem. M. S. Thesis. VPI., August 1965.

17. Hildebrand, F. B.: Advanced Calculus for Application. Prentice-Hall., Inc., Englewood Cliffs, New Jersey, 1962.

The vita has been removed from the scanned document

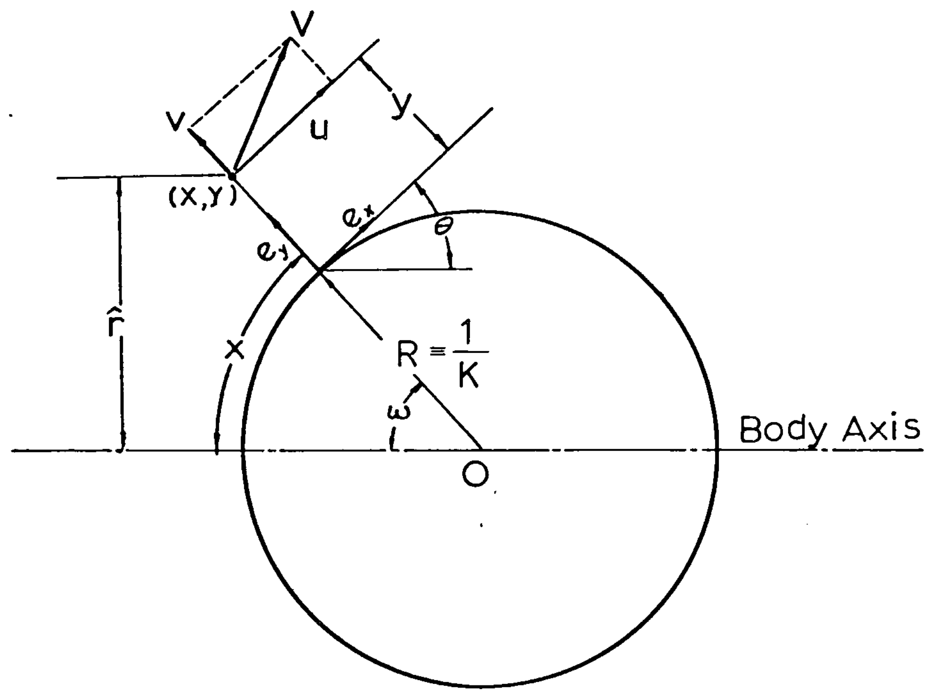

Figure 1. Body-Oriented Coordinate System of the Circular Cylinder

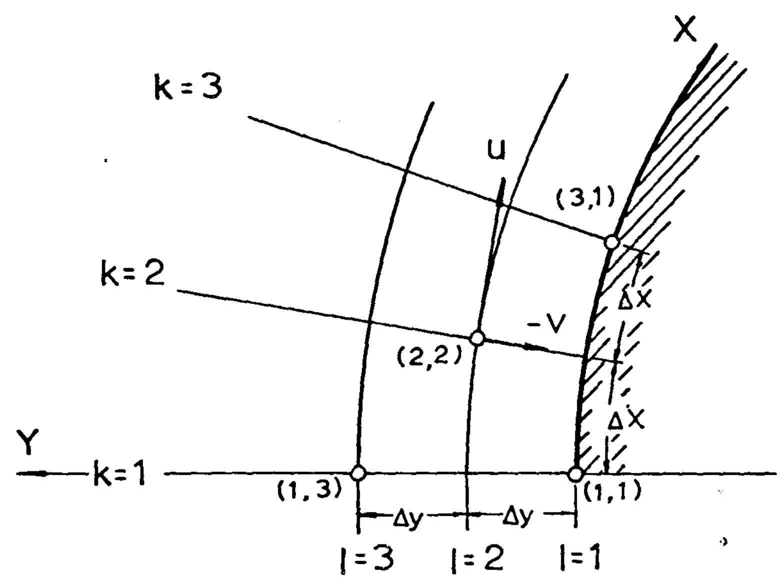

Figure 2. Mesh Spacing and Designation of Mesh Points in the Near Vicinity of the Body Stagnation Point

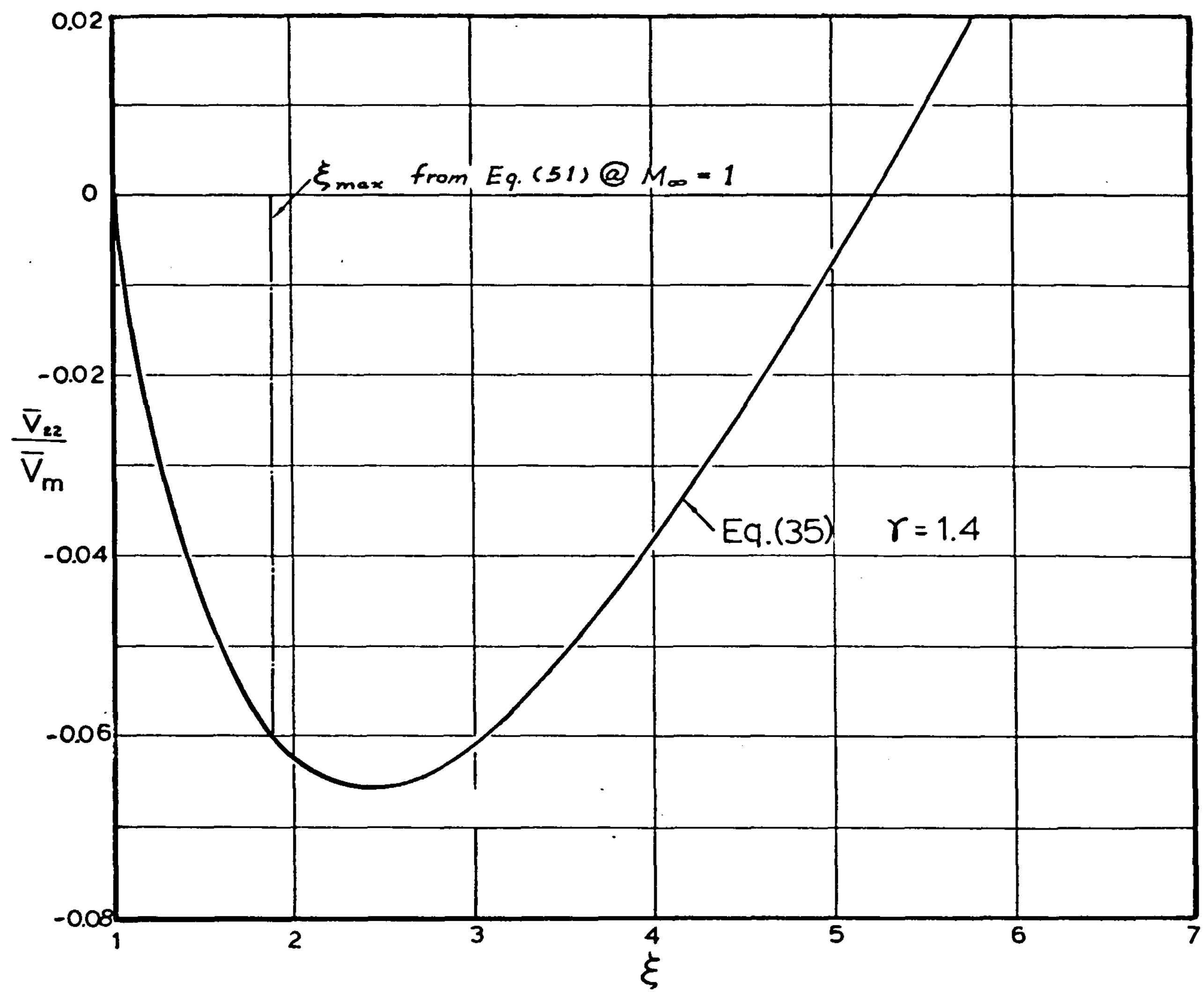

Figure 3. Variation of the v-Component of Velocity, $\bar{v}_{22}/\bar{V}_m$, at the Point (2,2) with the Pressure Ratio ξ

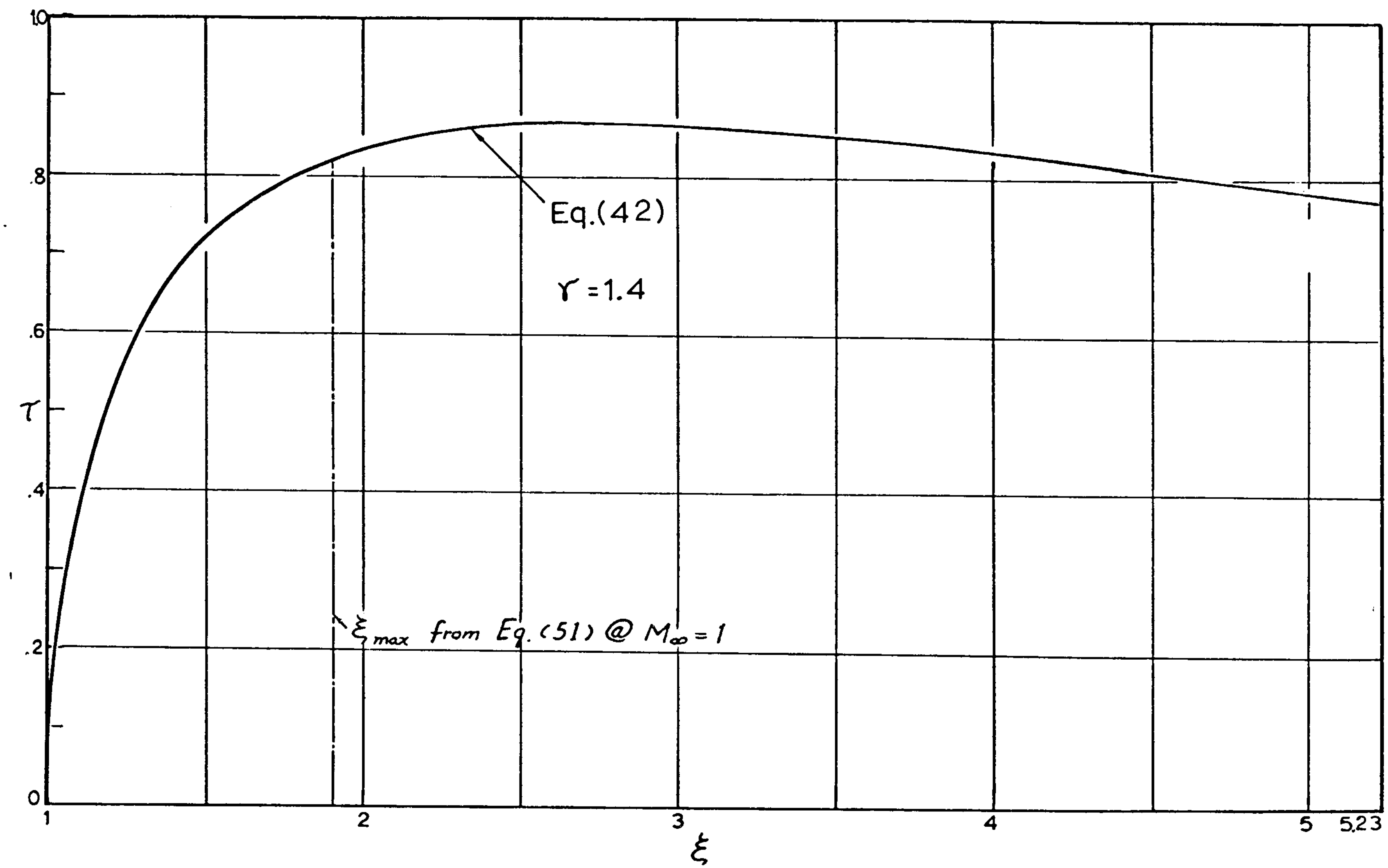

Figure 4. τ - ξ Boundary Curve

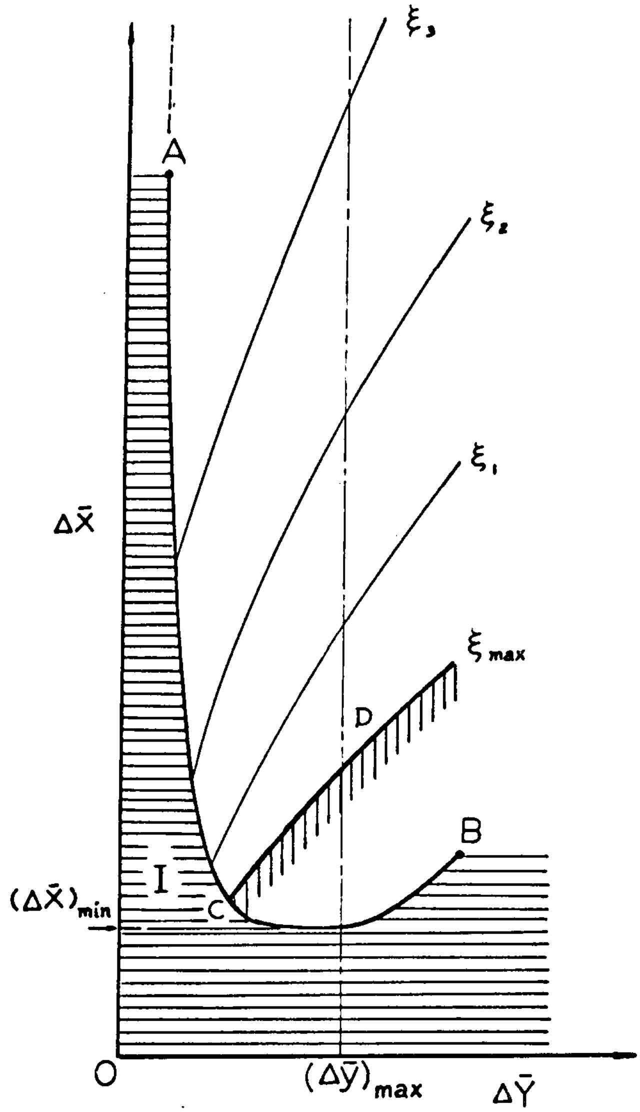

Figure 5. Representative $\Delta\bar{x}$ - $\Delta\bar{y}$ Plot Demonstrating the Boundary Between Real and Non-Real Solutions to the System of Difference Equations

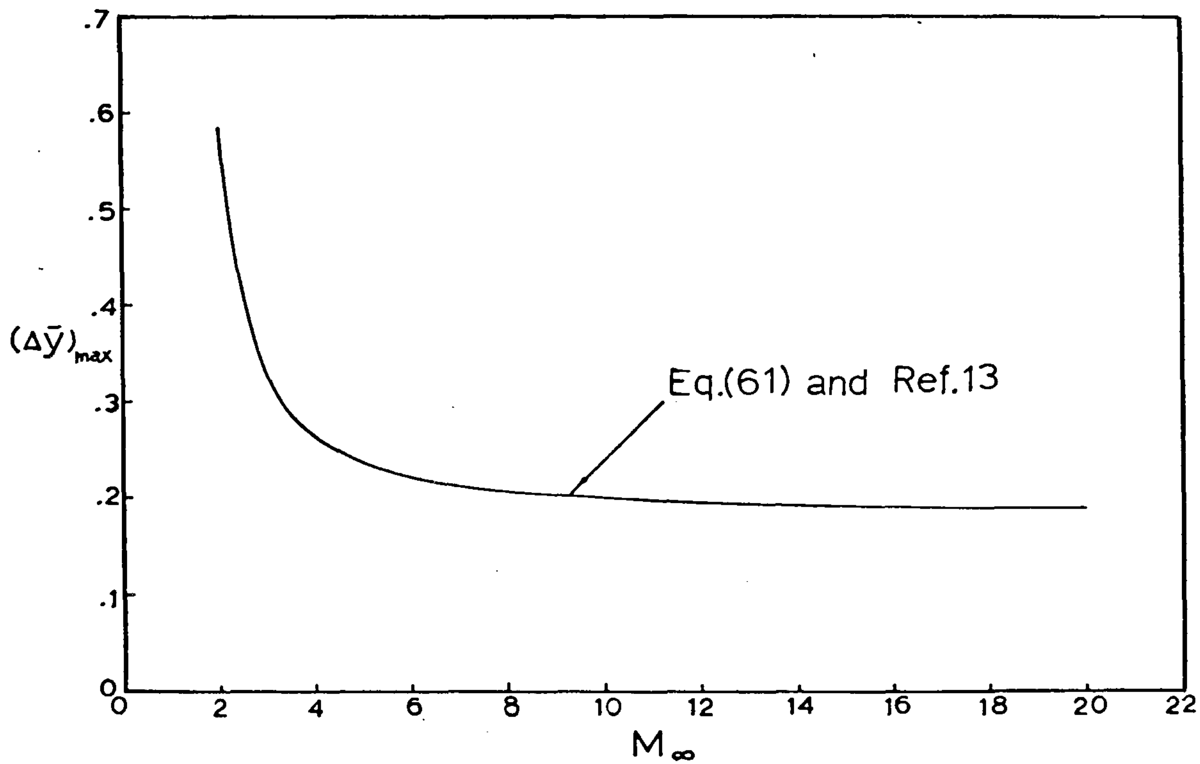

Figure 6. Values of $(\Delta\bar{y})_{max}$, as a Function of Freestream Mach Number, Based on Exact Theory

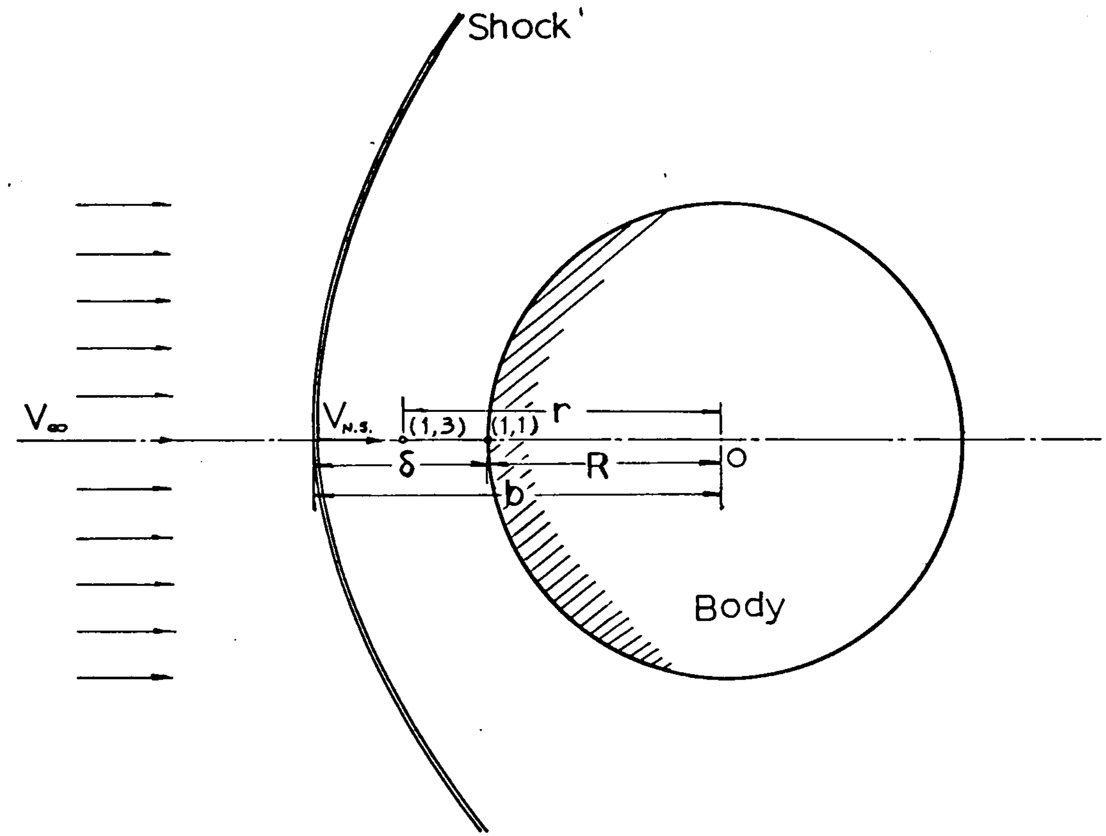

Figure 7. Orientation of the Bow Shock Wave and Stagnation Streamline for the Circular Cylinder in Supersonic Flow

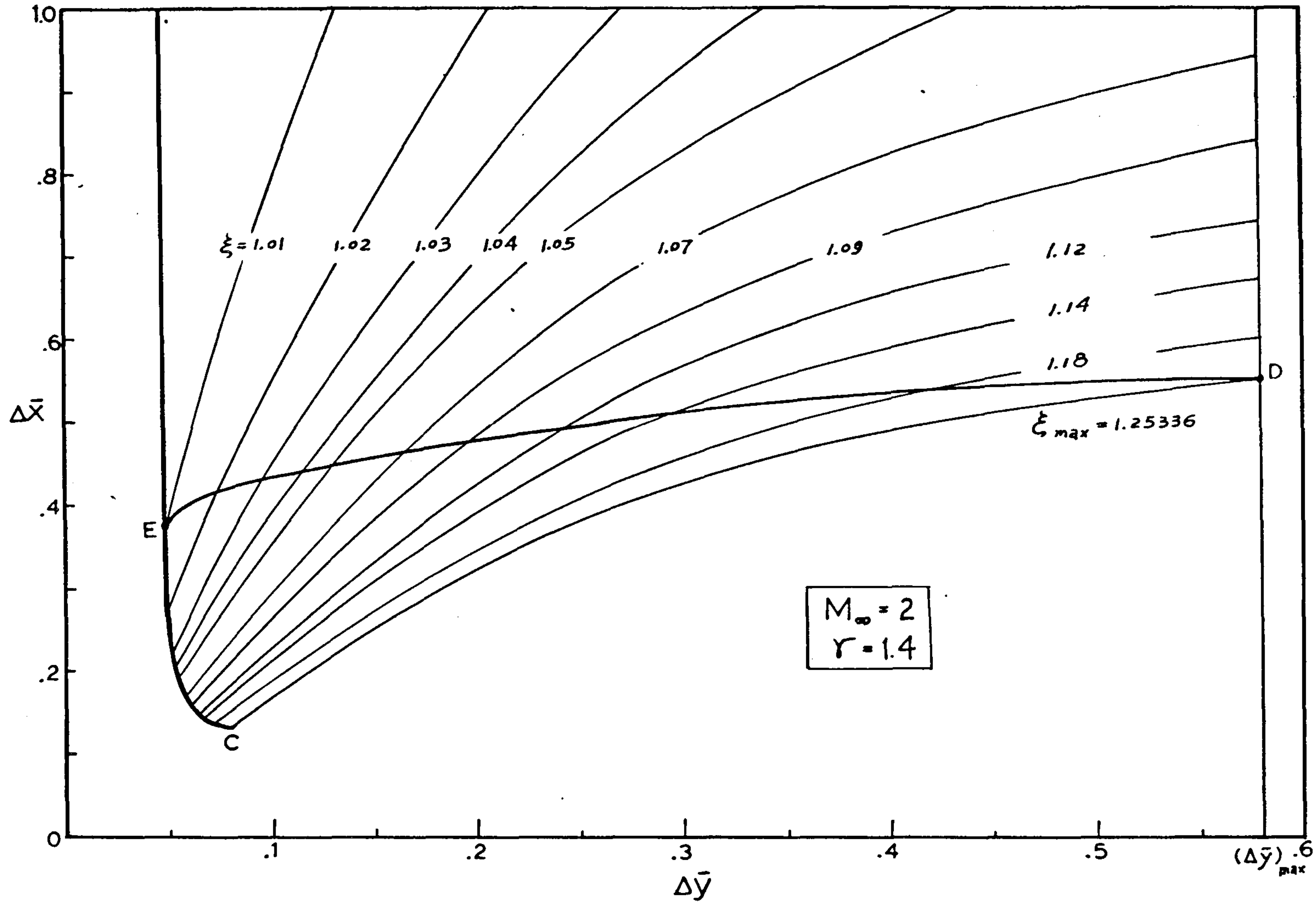

Figure 8. $\Delta\bar{x}$ - $\Delta\bar{y}$ Boundary Curve for M_∞ = 2

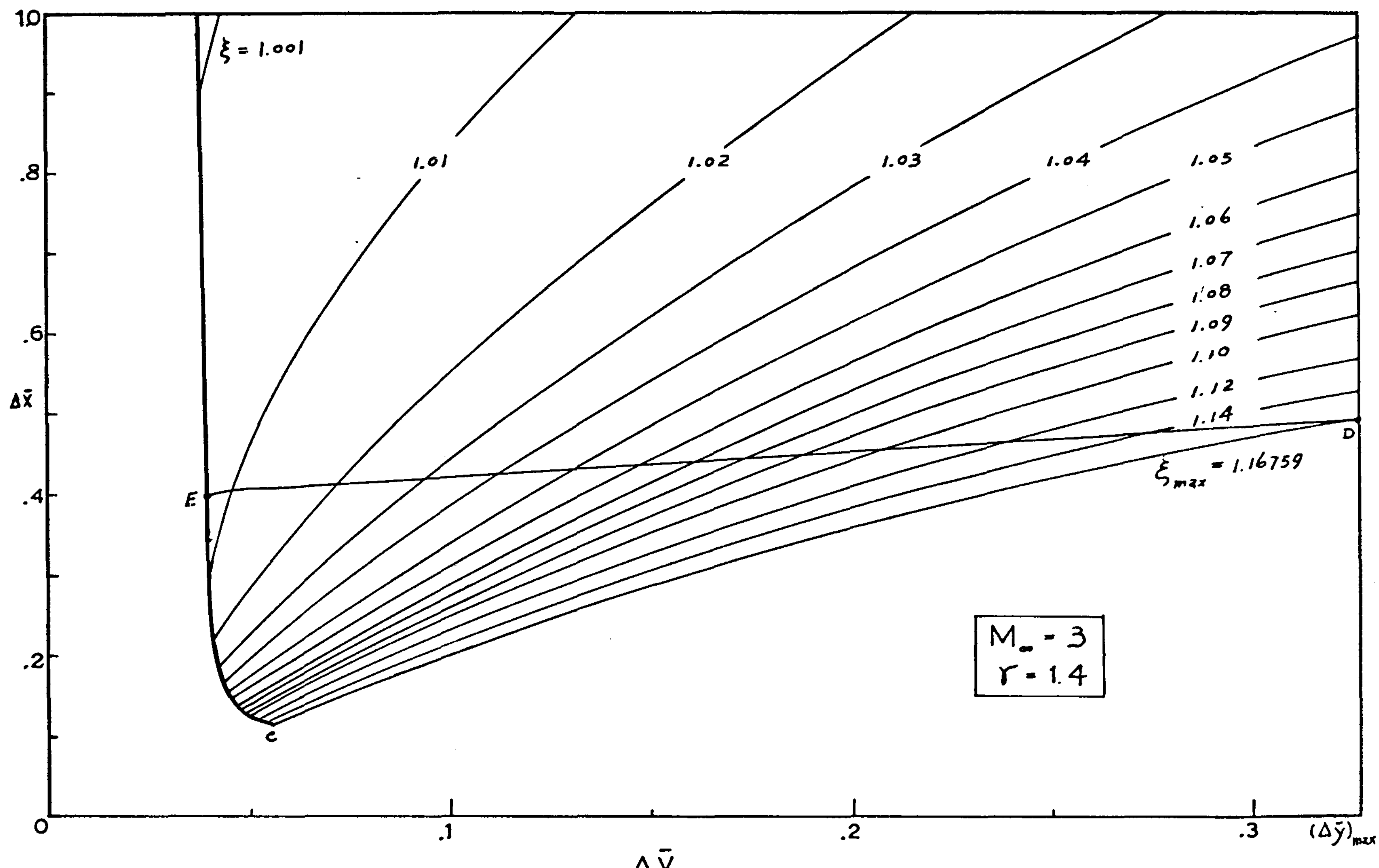

Figure 9. $\Delta\bar{x}$ - $\Delta\bar{y}$ Boundary Curve for $M_\infty = 3$

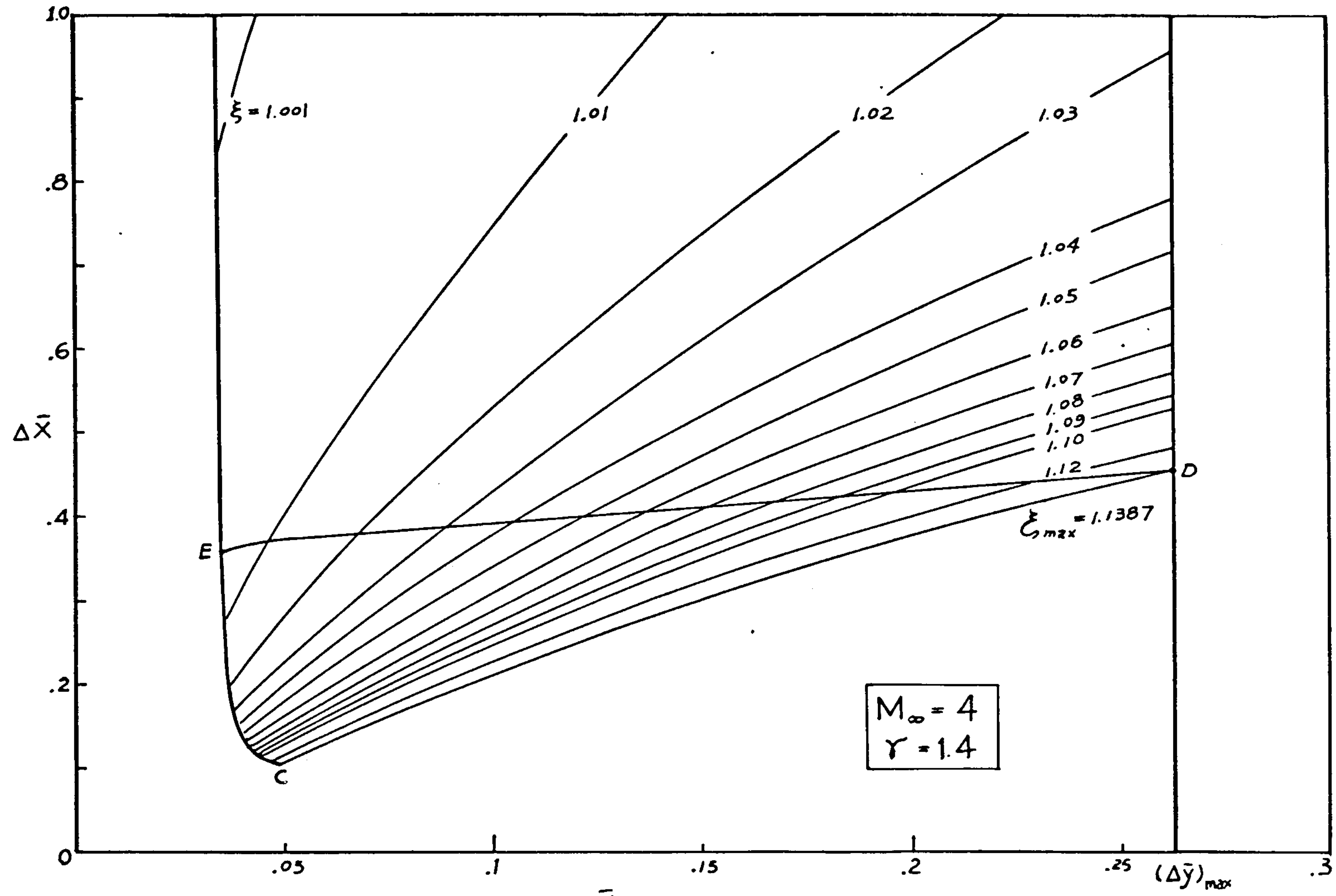

Figure 10. $\Delta\bar{x}$ - $\Delta\bar{y}$ Boundary Curve for $M_\infty = 4$

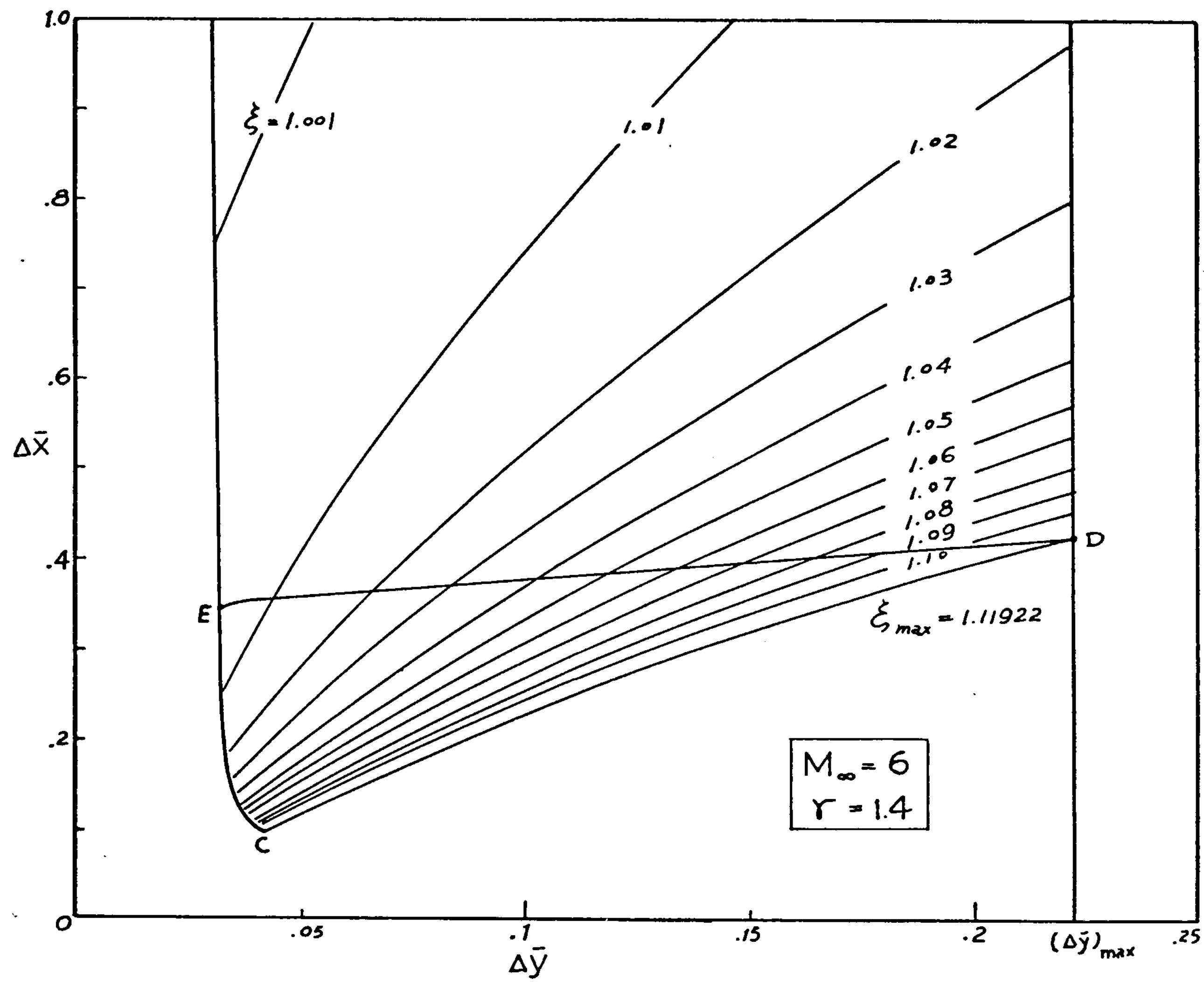

Figure 11. $\Delta\bar{x}$ - $\Delta\bar{y}$ Boundary Curve for $M_\infty = 6$

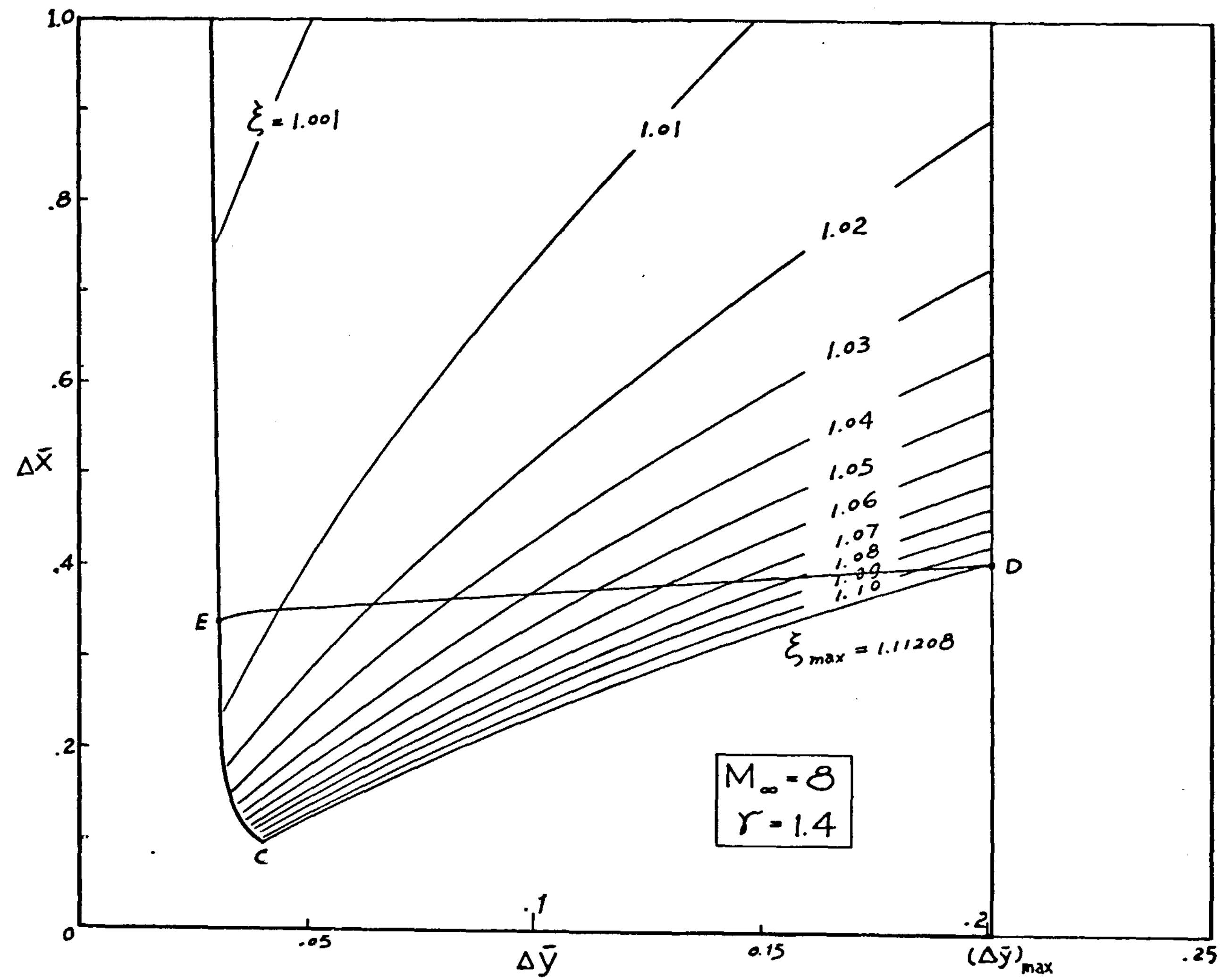

Figure 12. $\Delta\bar{x}$ - $\Delta\bar{y}$ Boundary Curve for $M_\infty = 8$

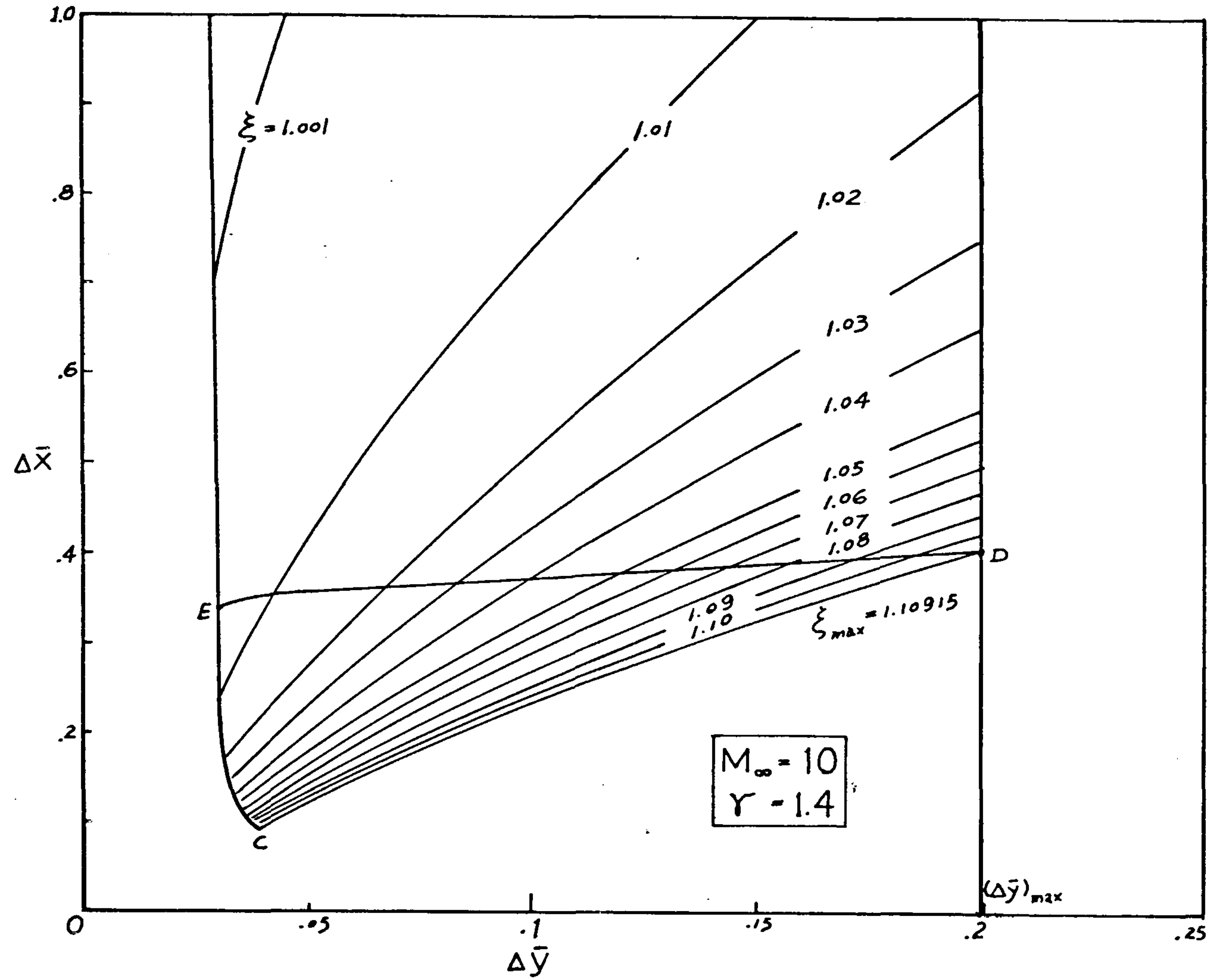

Figure 13. $\Delta\bar{x}$ - $\Delta\bar{y}$ Boundary Curve for $M_\infty = 10$

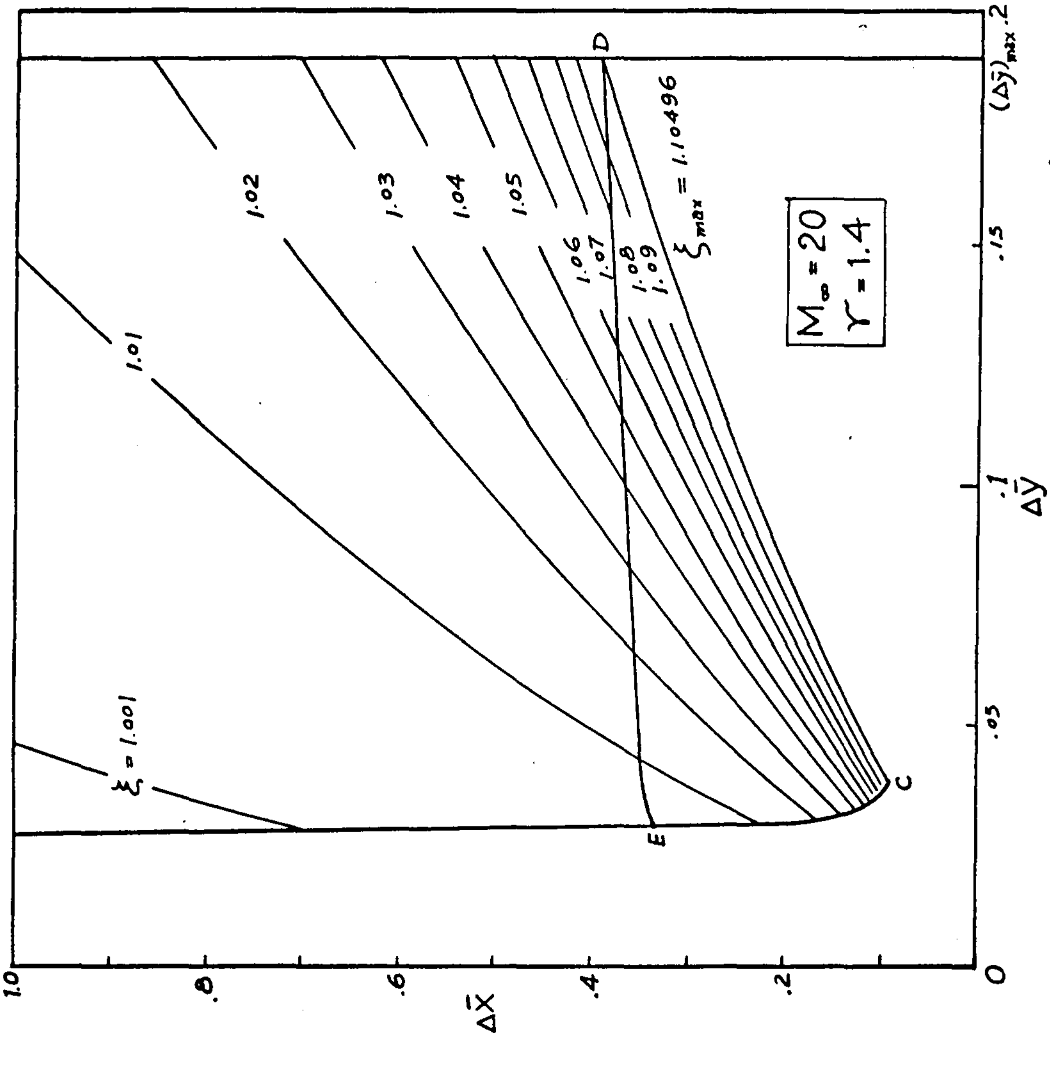

Figure 14. $\Delta\bar{x}$ - $\Delta\bar{y}$ Boundary Curve for M_∞ = 20

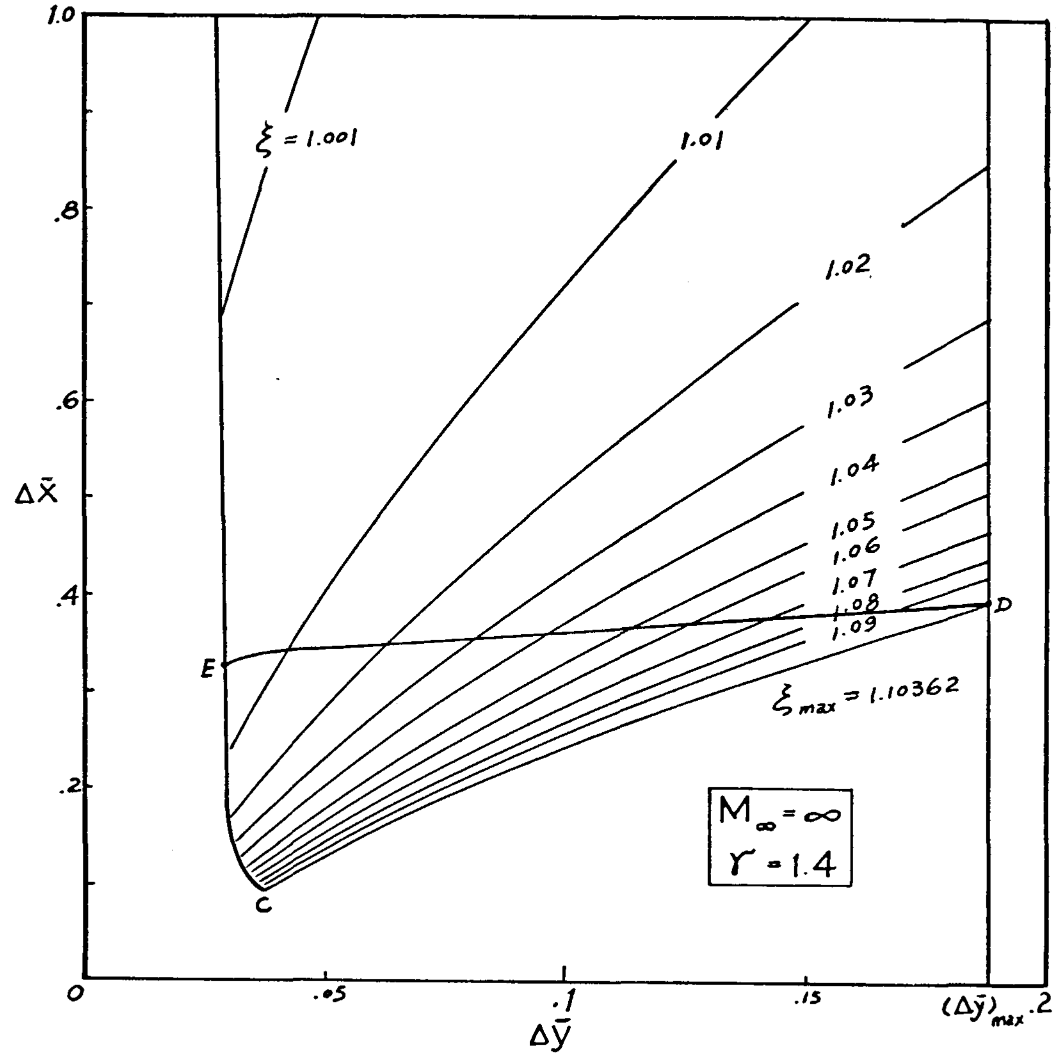

Figure 15. $\Delta\bar{x}$ - $\Delta\bar{y}$ Boundary Curve for $M_\infty = \infty$

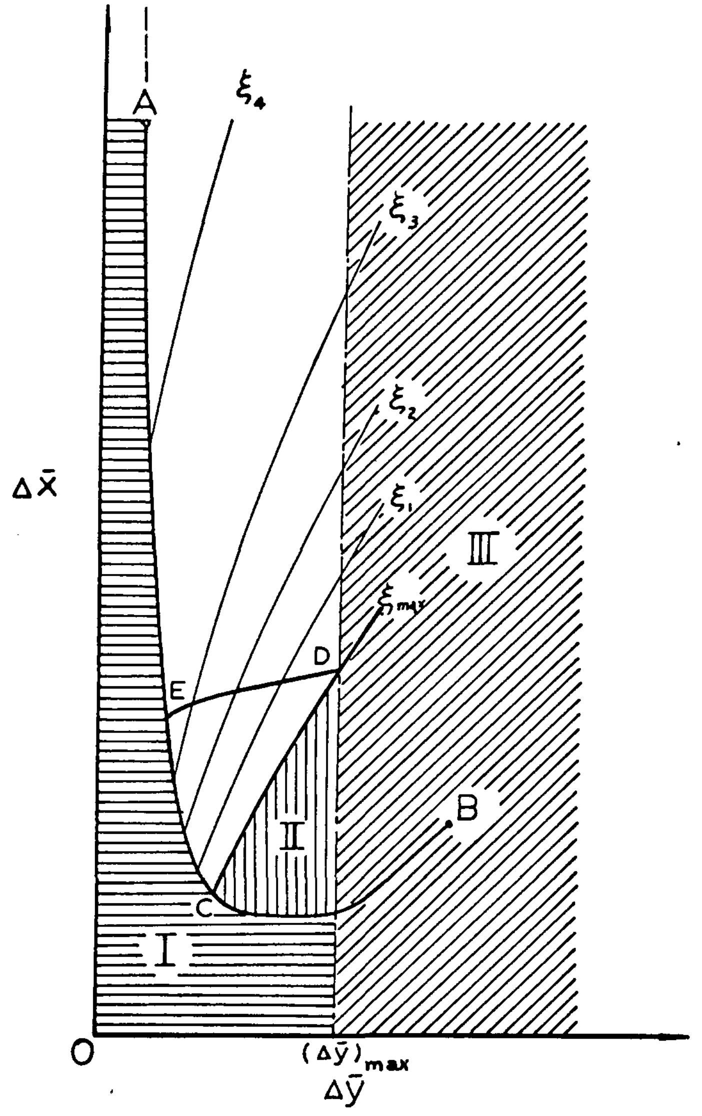

Figure 16. Restricted Region of Real Solutions in the $\Delta\bar{x}$ - $\Delta\bar{y}$ - ξ Domain

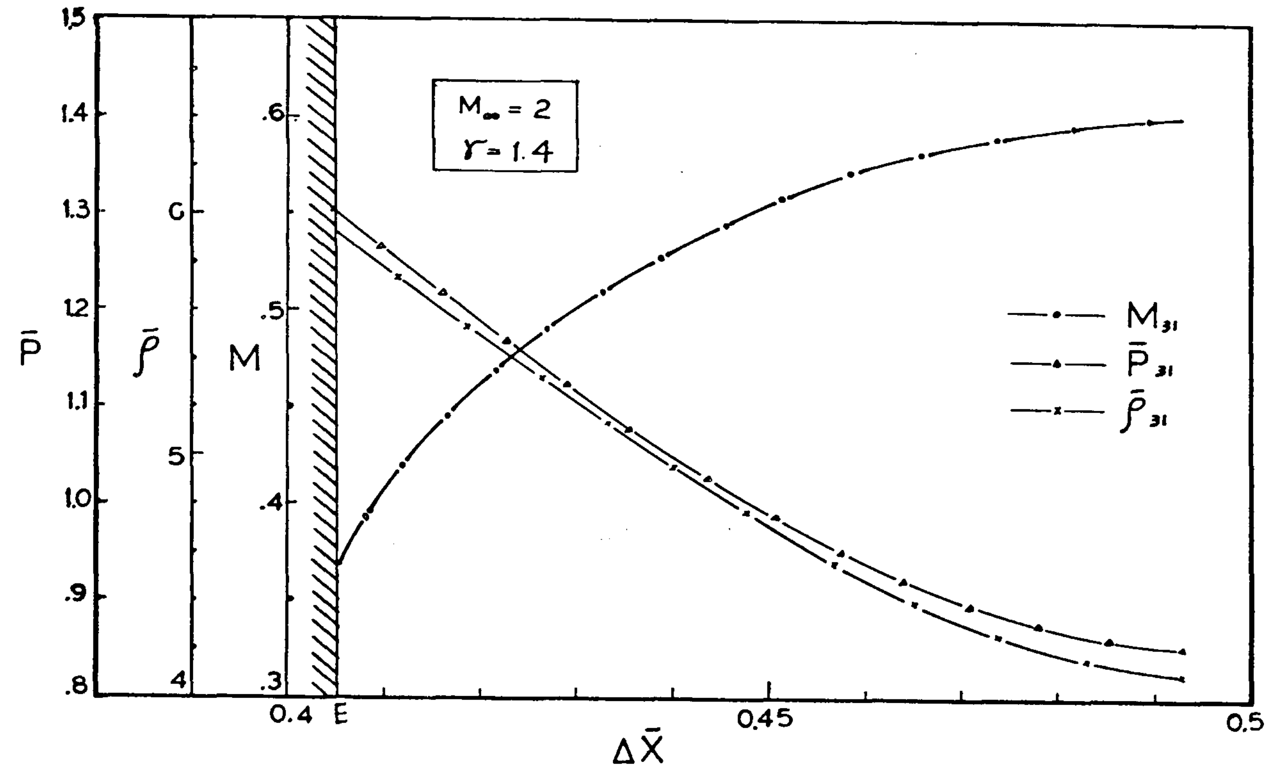

Figure 17. Variation of Local Flow Properties $\bar{P}$, $\bar{\rho}$, and M at Point (3,1) with Movement of the Point along the Body, $M_\infty = 2$

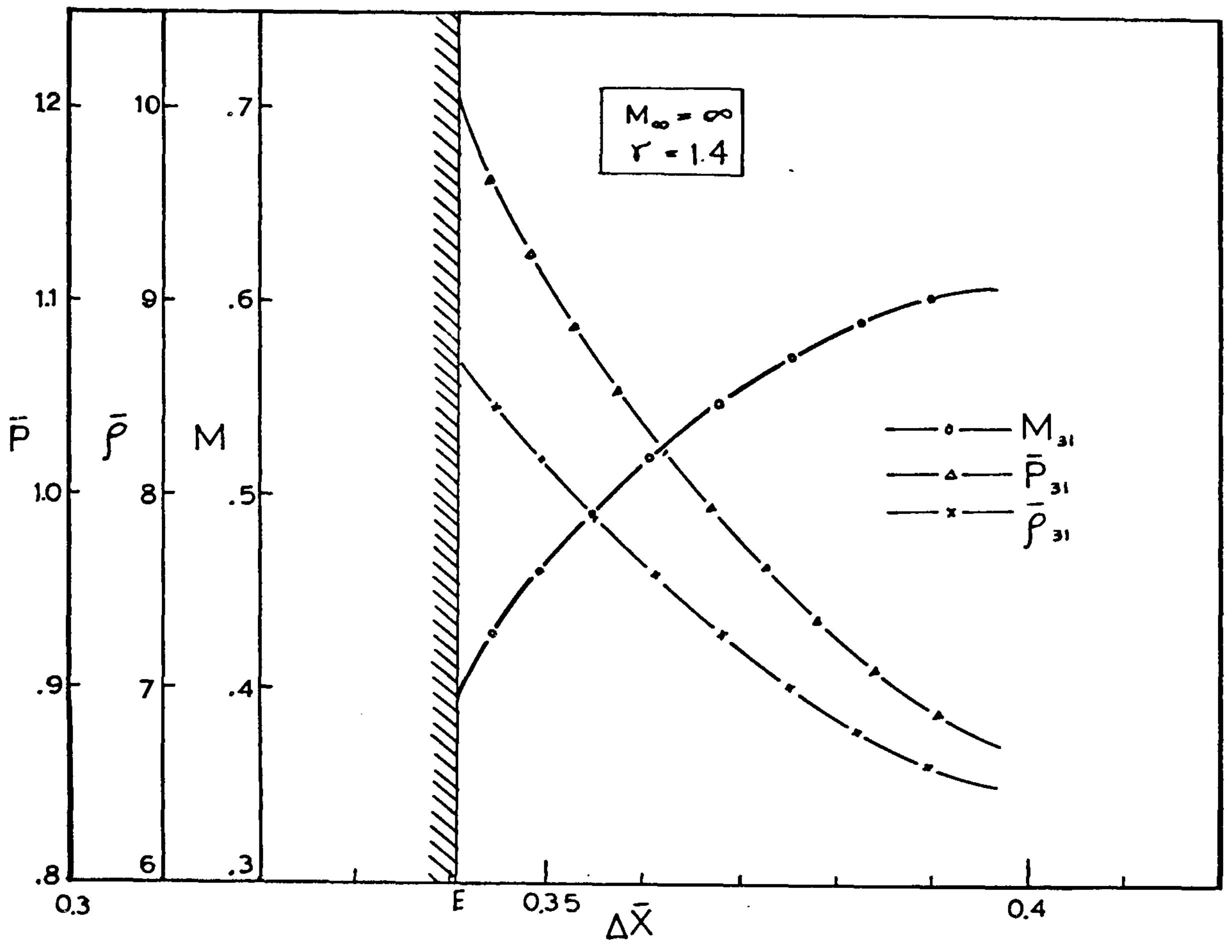

Figure 18. Variation of Local Flow Properties $\overline{P}$, $\overline{\rho}$, and M at Point (3,1) with Movement of the Point along the Body, $M_\infty = \infty$

AN ANALYTIC INVESTIGATION FOR SOLUTIONS OF FLOW PROPERTIES INSIDE THE SHOCK LAYER OF A SUPERSONIC FLOW PAST A CIRCULAR CYLINDER

by

Clarence Ming Chieh Chen

ABSTRACT

A finite difference method of investigating the shock layer in the vicinity of the stagnation point in a two-dimensional supersonic flow past a circular cylinder is analyzed. This method differs from existing methods which have been used in the past for solving this type of problem in that it uses the properties along the stagnation streamline as initial conditions. However, the method can still be classified as one of the direct type. A potential flow solution along the stagnation streamline is used to approximate the initial conditions. The results are compared with existing solutions and available experimental data.